의학박사 학위논문

자유롭게 움직이는 생쥐의 해마에서 sharp wave-ripple의 전기생리학적 신호와 칼슘 신호를 동시에 기록하는 방법과 활용

2023년 2월

서울대학교 대학원
의과학과 의과학전공
김채영

자유롭게 움직이는 생쥐의 해마에서 sharp wave-ripple의 전기생리학적 신호와 칼슘 신호를 동시에 기록하는 방법과 활용

지도 교수 김상정

이 논문을 의학박사 학위논문으로 제출함
2022년 10월

서울대학교 대학원
의과학과 의과학전공
김채영

김채영의 박사 학위논문을 인준함
2023년 1월

위 원 장	이용석	(인)
부 위 원 장	김상정	(인)
위 원	이석호	(인)
위 원	김명환	(인)
위 원	김선광	(인)

Simultaneous electrophysiological recording and calcium imaging of hippocampal sharp wave-ripple from freely behaving mice and the application

Supervisor Sang Jeong Kim

Submitting a Ph.D Dissertation of
Biomedical Science

October 2022

Graduate School of Medicine
Seoul National University
Biomedical Science Major

Chae Young Kim

Confirming the Ph.D Dissertation written by
Chae Young Kim
January 2023

Chair	Yong-Seok Lee (Seal)
Vice Chair	Sang Jeong Kim (Seal)
Examiner	Lee Suk-Ho (Seal)
Examiner	Myoung-Hwan Kim (Seal)
Examiner	Sun Kwang Kim (Seal)

Abstract

Simultaneous electrophysiological recording and calcium imaging of hippocampal sharp wave-ripple from freely behaving mice and the application

Chae Young Kim

Major in Biomedical Sciences

Department of Biomedical Sciences

Seoul National University Graduate School

Various experiences occur in our daily life in diverse context, and among them, some experiences become a life-long memory while some are easily forgotten. Not only encoding of experiences, this phenomenon of memory selection is heavily dependent on the consolidation of memory. In the investigation of long-term memory formation, hippocampal SWR signal and its neuronal contents have been extensively studied using neuronal decoding analysis of electrophysiological signal to recognize SWRs in the neuronal signals. However, as this signal has low spatial resolution and hard to track neurons across time, it has been difficult to analyze the individual contribution of neurons to task-specific SWRs.

In this work, I focused on the investigation of the hippocampal SWRs in spatial aspect not only in temporal aspect, and identification of cellular ensembles consisting of the activity to improve contents of consolidated memory by SWRs. To understand the composition of SWRs and its change by the environment in detail, I divided the research process into two parts.

In the first part, to investigate individual hippocampal neuronal activity participating in SWRs activity, I developed a Microdrive array with tetrodes, that combines with UCLA miniscope, a 1-p calcium imaging device. This method enables us to observe SWRs activity not only populational electrophysiological manner, as well as individual cellular activity using calcium indicators from freely behaving animals. The acquired data show that a group of hippocampal neurons was identified to have increased activity on the onset of SWRs, while activities were found to be decreased when SWRs are disrupted. This result implies the potential contribution of individual neuronal activity in the memory consolidation process.

In the second part, the calcium transient signals acquired from hippocampal neurons was compared by the environment of the animal. While animals are exploring two different environments, SWRs were detected in real-time and hippocampal neuronal activities were observed simultaneously. From the result, we found that different subsets of neurons are firing during SWRs depending on the environment of the animals, suggesting that SWR signals are collective signals of multiple neurons but their compositions are different by the contents of experience. This result has a potential to improve decoding accuracy when investigating replay contents and neuronal composition.

Overall, this thesis covers comprehensive strides from the development of tools to analysis of scientific findings in search of neuronal constitution of

memory engraved in the hippocampus.

(Keyword: learning and memory, hippocampus, local field potential, SWRs, tetrode recording, calcium imaging)

Table of contents

List of Figures and Tables

Chapter 1.

Chapter 2.

Chapter 3.

Chapter 1: Introduction

1. Learning and memory in the brain

1-1. Process of learning and memory

The learning and memory process is one of the most investigated topics in modern neuroscience. Learning refers to the process of acquiring new knowledge or skills, and memory is a process of storing acquired knowledge (Kandel et al., 2014). Learning and memory is a crucial function that allows organisms to cope with challenges in environments and adapt to a new one by changing behaviors (Maren, 2008). For example, recognizing the lack of food in the environment (learning) and adapting its behavior, i.e. looking for food or going out hunting, are based on the perception of external stimuli and previous experience for survival (memory).

The process of learning and memory involves several subcomponents (Figure 1.1). First, when external information is freshly acquired via neurons in sensory organs, it is stored in the prefrontal cortex as working memory or short-term memory. This short-term memory is volatile, easily forgotten, or reconstructed.

If the same information is repeatedly given, or spontaneously by internally occurring retrieval-mediated plasticity, labile memory is reinforced and stabilized. This reconstructed memory is transformed into another type of memory that lasts longer. This type of stabilized and more sustainable memory is called long-term memory. The process of transforming short-term memory to long-term memory is called memory consolidation, and it is stored in other regions of the brain such as the hippocampus. Memory

consolidation also serves to prolong the duration of long-term memory even longer, from hours to days or months, sometimes to life-long. In summary, memory consolidation is a process of stabilizing newly acquired information by abstraction (Xia et al., 2017, Joo & Frank, 2018, Roesler & McGaugh, 2019, Klinzing et al., 2019).

Memory retrieval refers to the recall of stored information, either automatically, or with certain stimuli (Frankland et al., 2019). When stored memory is accessible without cues, it is called recall. For instance, talking about the birthday party of last year, or taking writing tests are based on memory recall. When cues are necessary to identify stored memory that was previously experienced, it is memory recognition. One might not answer the correct answer on a writing test, but still could remember the correct answer on a multiple-choice test, using wrong choices as cues. Memory retrieval also takes place as a form of relearning, by unsettling previously stored memory (Frankland et al., 2013).

1-2. Memory classification

According to the memory model in Figure 1.1, it is largely classified into 3 categories: Sensory memory, short-term memory, and long-term memory (Figure 1.2).

Sensory memory is generated when external stimuli outside (visual, olfactory, tactile, etc) are perceived by an organism. This type of memory is stored to be further processed in the future even in the absence of the stimuli.

The other two forms of memory, short-term memory, and long-term memory are distinguished by the duration of availability for recall. Short-term

memory generally refers to the duration of seconds, minutes, or a few hours. Long-term memory refers to the memory that stays longer time span, often many hours, days, months, or even a life-long (McGaugh 1966).

Long-term memory is classified into two categories: declarative and non-declarative memory (Squire & Zola, 1996). Declarative memory refers to explicit memory, which is formed by the intentional recollection of prior information. There are episodic memory and semantic memory in declarative memory. Episodic memory refers to the recollection of total experiences, such as feelings and knowledge, from a specific place in time in the past. Semantic memory refers to rather pure knowledge without feeling in a specific background.

Non-declarative memory is also called implicit memory or procedural memory. This type of memory is not created or recollected with intention, but is formed unconsciously, and recalled automatically. Learning motor skills (i.e. riding a bicycle) or associated learning (i.e. Pavlovian conditioning) are representative examples of non-declarative memory.

The difference between short-term memory and long-term memory is well described in the study of patient H.M. by Scoville and Milner, reported in 1957. After an accident during childhood, H.M. suffered from minor sporadic seizures, which developed into major seizures as he grows up. When H.M. was 27 years old, his seizure was diagnosed to arise from medial temporal robe by W.B. Scoville, a neurosurgeon. H.M. was suggested to undergo experimental brain surgery dissecting bilateral medial temporal lobes, including anterior hippocampi, parahippocampal cortices, entorhinal cortices, piriform cortices, and amygdalae.

After the surgery, he did not have epileptic seizures anymore. However, he

started to develop severe anterograde amnesia and mild retrograde amnesia during his entire life. It was reported that he could remember events in the past years, but could not develop new long-term memory. He had a short working memory, but he could not have long-term memory, such as explicit or semantic memory (Scoville and Milner, 1957).

H.M.'s case suggests that different brain parts are involved in the memory process. Without the medial temporal robe, he still could have a short-term memory, but he could not recall it longer than a short moment, implying the role of the missing part of the brain in the development of long-term memory.

2. Structure of hippocampal complex

The hippocampus, a major part of the limbic system, is one of the major regions in the medial temporal lobe (MTL) of the brain. The MTL system is a fundamental region of declarative memory, whereas nondeclarative memory is supported by the striatum, amygdalam and cerebellum (Squire et al., 2004).

As a key structure of the brain, the hippocampus has many input and output connections. For instance, it supports communication between the subcortical structure and neocortex for memory consolidation and retrieval (Xia et al., 2017, Joo & Frank, 2018, Klinzing et al., 2019). In this section, I will overview the anatomical structure of the hippocampus and its communication with other regions from the perspective of memory formation.

2-1. Anatomical structure of hippocampus

The hippocampal system of rodents is composed of the hippocampus and

parahippocampal region (Figure 1.3, A). Hippocampus is also called Cornu Ammonis (Ammon's horn, CA) due to its horn-like shape connected bilaterally. It is divided into subregions including the dentate gyrus, CA 1, 2, 3, and the subiculum (O' keefe and Nadel, 1978, Eichenbaum and Cohen, 2001) (Figure 1.3, B). These subregions are morphologically distinct neuronal populations, and communication of each part is well-organized order of synaptic transmission.

Parahippocampal place area (PPA) refers to the surrounding region of the hippocampus and is divided into presubiculum, postsubiculum, postrhinal, perirhinal, and entorhinal cortices. This area is connected to the hippocampus directly and indirectly via the entorhinal cortex, providing processed information of external sensory stimuli (Furtak et al., 2007).

White matter fibers originating from the hippocampus are grouped to form a structure called the fornix. The fornix connects the hippocampus to other brain structures including the subcortical region, hypothalamus, and nucleus accumbens. Fornix from each hemisphere meets in the midline of the brain, and the fibers are partially intercrossed. This structure is called ventral hippocampal commissure (VHC) (Wyss et al., 1980). Since this structure is connected to the white matter layer of the hippocampi in both hemispheres, it is widely used to investigate the function of hippocampal LFP from freely behaving animals using electrical stimulation (Ego-Stengel et al., 2010).

2-2. Internal computation in the hippocampus

As a hub of the memory system of the brain, the hippocampus receives many direct and indirect inputs from diverse parts of the brain. One

representative input to the hippocampus is from the neocortex.

When external information of an organism is processed in the sensory cortices, the processed signal is sent to the parahippocampus (peri- and postrhinal cortices), which is eventually sent to the entorhinal cortex. This processed information is sent to the dentate gyrus of the hippocampus via the perforant pathway, which is known to be critical for spatial working memory and novelty detection (Vago and Kesner, 2008).

The signals from the dentate gyrus are sent to CA3 via mossy fibers and the axon of CA3 projects to CA1 via Schaffer collaterals. Schaffer collateral has been used as a sample synapse to generate long-term potentiation (LTP) of the hippocampal formation, which is important for activity-dependent plasticity for learning and memory (Moretti et al., 2006).

Axon of CA1 pyramidal neurons innervates to the subiculum, which is the main output of the hippocampus. It directs to diverse brain regions, including the entorhinal cortex in the parahippocampus (Figure 1.3, C)

2-3. Interaction of the hippocampus with other brain structures

The main output structure of the hippocampus is the subiculum (O' Mara, 2005, Matsumoto et al., 2019). Via subiculum, internally computed hippocampal signals are transmitted to the thalamus, hypothalamus, amygdala, nucleus accumbens, orbitofrontal cortex, ventromedial nucleus, septal complex, and more (Van Strien et al., 2009, Strange et al., 2014).

Hippocampus has bidirectional interaction with the prefrontal cortex which is

well known for its complementary function of episodic memory, spatial memory, as well as memory consolidation and retrieval (Scoville & Milner, 1957, Wang & Morris, 2010, Vann et al., 2011, Preston & Eichenbaum, 2013, Moscovitch et al., 2016, Eichenbaum, 2017, Xia et al., 2017, Joo & Frank, 2018, Klinzing et al., 2019, Sirota et al., 2003). It has been reported that disrupted PFC–hippocampal interaction is found in schizophrenia patients and animal models of the disease, implying its critical role in memory, cognitive functions such as decision–making, and behavioral control (Anderson et al., 2016, Sigurdsson & Duvarci, 2016).

The entorhinal cortex (EC) is also of major projection from the hippocampus, as well as an input. Internally processed information from the hippocampus is sent to EC via subiculum. For instance, spatial representation of self is demonstrated by grid cells in EC, which is assumed to bidirectionally cooperate with place cells in the hippocampus, for accurate coding of self in large–scale spatial metric (Hafting et al., 2005, Fyhn et al., 2007, Ahmed & Mehta, 2009, Bush et al., 2014, Dordek et al., 2016).

Studies revealed that activated innervation of the amygdala to hippocampal CA1 can control both positive and negative emotions such as anxiety, social behaviors, as well as emotion–modulated spatial memory (Tottenham & Sheridan, 2010, Yang & Wang, 2017). Nucleus accumbens is also known to interact with the hippocampus for reinforcement learning and context conditioning via dopamine pathway or synaptic plasticity (Packard & McGaugh, 1996, Ito et al., 2008, Abela et al., 2015, Legates et al., 2018, Duncun et al., 2018). Hypothalamus, ventral tegmental area (VTA), locus coeruleus (LC), and septum also send inputs to the hippocampus, implicating in novelty perception, attention, and spatial memory (Lisman & Grace, 2005, Khakpai et

al., 2013, McNamara et al., 2014, Takeuchi et al., 2016, Burdakov & Peleg-Raibstein, 2020, Chen et al., 2020).

3. Hippocampal SWR and memory

3-1. Pyramidal neurons in the hippocampus

A pyramidal cell is a type of excitatory neuron with a cell body in a triangle shape (Figure 1.5 C). It is the most populous cell of the excitatory neuron family that exists in various species, including mammals. In rodents, it is found in the hippocampus, and amygdala, and consists of two-thirds of neurons in the cerebral cortex, suggesting its importance in the cognitive process (Spruston, 2008, Bekkers, 2011).

In the hippocampus, pyramidal neurons are distributed heterogeneously over the principal circuitry (dentate gyrus (DG)-CA3-CA1). In rodents, the firing rate of regular pyramidal neurons lies between 0.1-10 Hz, either in resting state or active running state *in vivo* (Hirase et al., 2001), but *in vitro*, there is a regular spiking as well as burst spiking (100-300Hz) (Figure 1.5, A, B) (Graves et al., 2012, Okamoto et al., 2014). In CA1, while the majority of pyramidal cells are silent, firing patterns of some neurons are found to be selective to the spatial location of the self, which is called place field, and the neuron is called place cell (O'Keefe & Dostrovsky, 1971). This particular firing pattern of neurons is known to be controlled by excitation-inhibition balance by input from CA3 and the entorhinal cortex (Ahmed & Mehta, 2009). Their firing pattern also can change depending on the environment, experiences, as well as behavioral states (Hirase et al., 2001, Sirota et al., 2003, Peigneux et al., 2004).

3-2. Hippocampal LFP and Sharp Wave-Ripples (SWRs)

In vivo recording of the hippocampus in freely behaving rodents allows observing electrophysiological data consisting of a neuronal population of interest, which is called local field potential (LFP). In the hippocampus, there are 2 distinctive LFP signals depending on the states of behavioral activity.

One of them is large irregular activity (LIA), which appears during pauses, sleep, especially slow-wave sleep (SWS) states (Buzsaki, 2015). It is terminated by Vanderwolf in 1969, describing small and irregular activity states interweaved in predominantly lower oscillation frequency signals. These transient (50-120ms) and fast (140-225Hz) spikes are called sharp waves, and the large oscillatory signals with sharp waves are called sharp wave-ripples (SWRs) (Figure 1.6) (Buzsaki, 1986, Buzsaki et al., 1992, Jarosiewicz et al., 2002, Colgin, 2016). Besides the hippocampus, SWRs have been reported to be observed in the rhinal cortex (Chrobak and Buzsaki,1996), amygdala (Ponomarenko et al., 2003; Haufler and Pare., 2014), and endopiriform nucleus (Ponomarenko et al., 2003) in rodents. In humans, SWRs with a slower frequency of ripple (~80Hz) have been observed not only in the hippocampus (Staresina et al., 2015), but also in the neocortex (Norman et al., 2019; Vaz et al., 2019), rhinal cortex (Staba et al., 2002), and the amygdala (Cox et al., 2020).

On the other hand, in running or active awake states, the LFP of hippocampal CA1 regions is approximately 6-8Hz theta oscillation. It is known to arise from the interaction between the septum and hippocampus. Theta oscillation in the hippocampus is known for its function in timing mechanism to

temporally organize movement sequences, memory processing including encoding, as well as planned trajectories for spatial navigation (Jacob et al., 2014; Kragel et al., 2020; Nunez & Buno, 2021).

3-3. SWRs, replay and memory consolidation

In the field of sleep studies, previous research focused mostly on the REM sleep phase. However, recent sleep studies pay more attention to the SWS phase during which SWRs activity occurs.

In the learning and memory process of an organism, the labile memory trace is gradually stabilized by consolidation processes. A number of studies hypothesized and suggested that long-term memory is formed by an active consolidation process during sleep, which is the reactivation of newly encoded memory representations (Rasch & Born, 2008; Diekelmann & Born, 2010; Ellenbogen et al., 2007; Lewis & Durrant, 2011). These repeated reactivations occur during SWS, while the reactivated memories are stabilized during REM sleep (Rasch & Born, 2013; McGaugh, 2000). Not only in rodents but this function of SWS in memory consolidation was also studied in clinical research (Peigneux et al., 2004; Takashima et al., 2006; Marshall & Born, 2007; Schonauer et al., 2017).

Currently, the principle behind the memory consolidation of short-term memory to long-term memory by SWRs is explained by spindle-ripple coupling between hippocampus and PFC (Girardeau & Zugaro, 2011; Xia et al., 2017; Shin et al., 2019; Ngo et al., 2020). It also has been reported that the effect of SWRs on memory performance varies depending on their duration (Fernandez-Ruiz et al., 2019; Ngo et al., 2020). Not only memory

consolidation, but SWRs have also been reported to be related to memory retrieval (Colgin, 2016; Joo & Frank, 2018; Norman et al., 2019; Schreiner et al., 2021).

3-4. SWRs and hippocampal replay

In the hippocampus, reactivation of neuronal sequences was observed sequentially and consistently while animals are in sleep, rest, or stationary position, (Wilson & McNaughton, 1994; Ji & Wilson, 2007; Skaggs & McNaughton, 1996), or during mobility (Diba and Buzsaki, 2007; Foster and Wilson, 2006). In the case of place cells, re-activation sequences are faster than during experience. This sequential activation of neurons is called hippocampal replay. A neuronal replay of the encoded memory representation is found to be repeated during SWS sleep, driving concrete short-term memory in the neocortical network to be transformed into abstract long-term memory (Lewis & Durrant, 2011; Klinzing et al., 2019). This replay is known to be accompanied by SWRs (Kudrimoti et al., 1999; Diba & Buzsaki, 2007).

Re-expression of neuronal sequences could occur in either a forward direction or reverse direction, which is called forward replay and reverse replay, respectively. In place cells, these two types of replays are known to have different functions. For instance, it was reported that forward replay is to reactivate encoded neurons for memory formation, and reverse replay is for planning for future direction (Diba & Buzsaki, 2007; Gupta et al, 2010; Carr et al., 2011).

In replay research of place cells, this reactivation of neuronal sequences is found to anchor to the current location of the animal. However, some studies

also reported that replays with shorter duration were observed in distant places (Pfeiffer & Foster, 2013; Davidson et al., 2009). It was also observed that during SWRs, sequenced reactivation of neurons representing location appears discontinuously, implying intermingled events of replay and retrieval phases (Pfeiffer & Foster, 2015).

3-5. The engram

Since the replay phenomenon has been observed, there has been another question: what are these re-activated neurons? Why are they firing in sequence but not others? One interpretation of this selective neuronal activation in the sequence is that these particular neurons encode information from the outer world and store memory exclusively for others. The concept that memories are stored only in selective neurons is called engram theory, and the related are called engram cells (Liu et al., 2012).

This idea was advanced thanks to the development of genetic tools using the tTA-TetO system, which allows to tag group of neurons activated by certain experiences (Josselyn et al., 2015). Using this method, the memory engram was found not only by previous experiences but also by false memory (Diekelmann et al., 2010, Liu et al., 2012) or even in animals with amnesia (Ryan et al., 2015). The selection mechanism of engram cells could be explained by intrinsic excitability or synaptic plasticity between neurons (Josselyn & Tonegawa, 2020). Currently, the engram cells are understood as a substrate of memory (Tonegawa, et al., 2015, Josselyn et al., 2015).

4. Technologies to monitor chronic extracellular neuronal activity in vivo

Roles of hippocampal SWRs activities are often investigated using behavioral tasks of the animal. In this section, I introduce in-vivo recording technologies used to acquire hippocampal neuronal activities applied to freely behaving animals in behavioral tests.

4-1. Electrophysiology

1) Electrode wires with Microdrive array

Tetrode is an electrode consisting of 4 twisted tungsten wires (Gray et al., 1995, Davidson et al., 2009, Chen et al., 2017). Each wire of tetrode is able to record an electrical signal from a neuronal population in the local region of the brain. As it is composed of 4 wires, it is also possible to estimate a relative spatial location of neurons among the recorded field potential of the population, which is useful for decoding the signal. Tetrode recording for rodents is often performed by a Microdrive array to control recording depth as well as acquire signals from a large population. Microdrive arrays are designed to carry tetrode in diverse shapes, for the purpose of recording and shape of the target brain region.

Hippocampal SWRs are a very fast and transient LFP activity, which needs to be recorded using an electrophysiological manner to preserve its temporal precision. SWRs are often recorded in CA1 of the hippocampus which has a long and flat structure along the axis of the hippocampus. Therefore, to record SWRs using tetrode, a Microdrive array could be an ideal method to cover a

flat surface with a group of electrodes next to each other. Once the drive is implanted in the hippocampus, each tetrode is individually inserted to reach the target layer and collect the LFP signal (wide band, 0.01−6000Hz). Collected signals are filtered to the ripple band (140−225Hz) and the onset, duration, and frequency of SWRs are monitored from freely behaving animals.

2) Silicon probes with electroplate

Silicon probe is a more recently developed electrophysiological method for LFP recording (Harris et al., 2003, Csicsvari et al., 2003, Ber□nyi et al., 2014, Pesaran et al., 2018, Allen et al., 2019, Hong & Lieber, 2019). The initial design is a linear shape with metal recording plates, but depending on the purpose of research, there are various choices of design, material as well as a combination of other tools such as fibers for optogenetics or micro−infusion of a drug (Takeuchi et al., 2003, HajjHassan et al., 2008, Buzsaki et al., 2015, Chen et al., 2017). Since there is a bigger number of recording sites in the silicon probe and it can cover a larger area of the brain depending on its shape, it is more favorable to recognize the spatial location of neurons, such as recording multiple layers of the neocortex. However, although it is more efficient to collect signals from a larger population of neurons, it might not be an ideal method to record SWRs signals in the hippocampus, as it is more appropriate for the ventral−dorsal directional structure of the brain than the laterally flat structure like the hippocampus.

4−2. Calcium imaging

When neurons are activated and generate action potentials, intracellular calcium level increases. The principle of the calcium imaging technique is to detect intracellular calcium using attached fluorescent molecules and to observe the spontaneous activity of intact neurons. As the kinetics of intracellular calcium concentration is relatively slow, the temporal resolution of the neuronal signal is lower compared to the electrophysiological technique and not sufficient to record local field potential. However, unlike tetrode or silicon probe recording which acquires a sum of signals from large population neurons without spatial precision, the calcium imaging technique can provide signals from individual neurons with high specificity over a large field of view.

Calcium imaging techniques are broadly divided into 1-photon or multi-photon depending on the number of photons used for the data acquisition method.

1) Miniscope imaging

Among many 1-photon imaging techniques, miniscope imaging is one of the most recently developed techniques in neuroscience for calcium imaging *in vivo* (Figure 1.12, A) (Cai et al., 2016, Aharoni et al., 2019, Resendez et al., 2016, de Groot et al., 2020). Compared to multi-photon imaging methods, it is broadly used to observe neuronal activity during behavioral tasks from freely behaving animals, thanks to its light weight, adaptability as well as budget-friendliness. To reduce cost and weight, instead of a laser, LED is used as a source of light. When the LED light is shed on the target brain region through implanted GRIN lens (GRadient INdex lens), emitted light from neurons is collected and projected to the CMOS sensor through the GRIN lens

(Figure 1.12, B). Acquired signals are displayed in real-time from freely behaving animals.

Since it uses only one source of light using LED, the resolution is relatively lower than the multi-photon imaging technique. However, it has a larger field of view (FOV) with more observable neurons from a single imaging plane. Also, it is light and easy to attach and detach to the brain of the living animal, it is an optimal tool for recording spontaneous and individual neuronal activity from freely behaving animals combined with behavioral tests. Moreover, the implanted lens enables keeping a tract of the identical neuronal population over a long period, which is an ideal tool to investigate the change of neuronal activity throughout elapsed time or as a result of specific behavioral training. The acquisition frame rate (Frames per second, FPS) is 30Hz, which is suitable for imaging hippocampal pyramidal neurons whose general firing frequency is around 1Hz at rest and up to 20Hz at during activity (Wiener et al., 1989, Czurko et al., 1999, Hirase et al., 1999)

2) Multi-photon imaging

Multi-photon imaging techniques are also used for recording neuronal activity in the brain in vivo. Unlike 1-photon calcium imaging, it uses multiple light sources to precisely target a particular area or neurons in the population.

To image the deep region of the brain, it is necessary to excite tissue by wavelength with higher energy. And the power of the photon is inversely proportional to the wavelength of light. Therefore, exciting brain tissue using photons with too high energy is likely to damage neurons, which does not allow long-term and spontaneous neuronal recording. On the other hand,

two-photon microscopy uses 2 photons from a high wavelength for an exciting fluorophore, which induces less damage in deeper brain regions. Further, two photons enable imaging of neuronal populations with higher spatial precision and even specifically target single neurons for excitation (Emiliani et al., 2015, Marshel et al., 2019, Russell et al., 2022).

Recently, three-photon microscopy (3PEF) is also being developed. Advanced from two-photon microscopy, 3PEF uses 3 exciting photons to target deeper tissue. It can image deeper regions without scattering, still with a high-resolution fluorescent signal of neurons (Wang and Xu, 2020, Sinefeld et al., 2022).

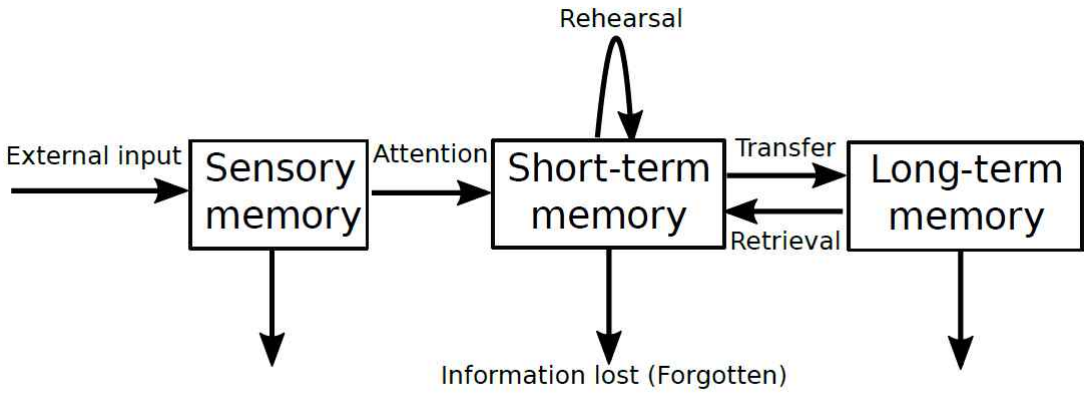

Figure 1.1. Atkinson & Shiffrin's multi-store memory model. Memory consisted of three stores (sensory memory, short-term memory (STM), and long-term memory (LTM)). External sensory input is constantly encoded in sensory memory for a very short time, but most of them receive no attention. When it receives attention, it is stored as STM in a large capacity but for a very brief duration (up to 30 seconds). If rehearsal occurs continuously, the information is getting a stronger memory to be an LTM. Without continuous rehearsal, STM is decayed and forgotten. LTM has unlimited duration and capacity. Rehearsal involves the process of linking new LTM to information already stored in LTM. (Adapted from Atkinson & Shiffrin, 1968).

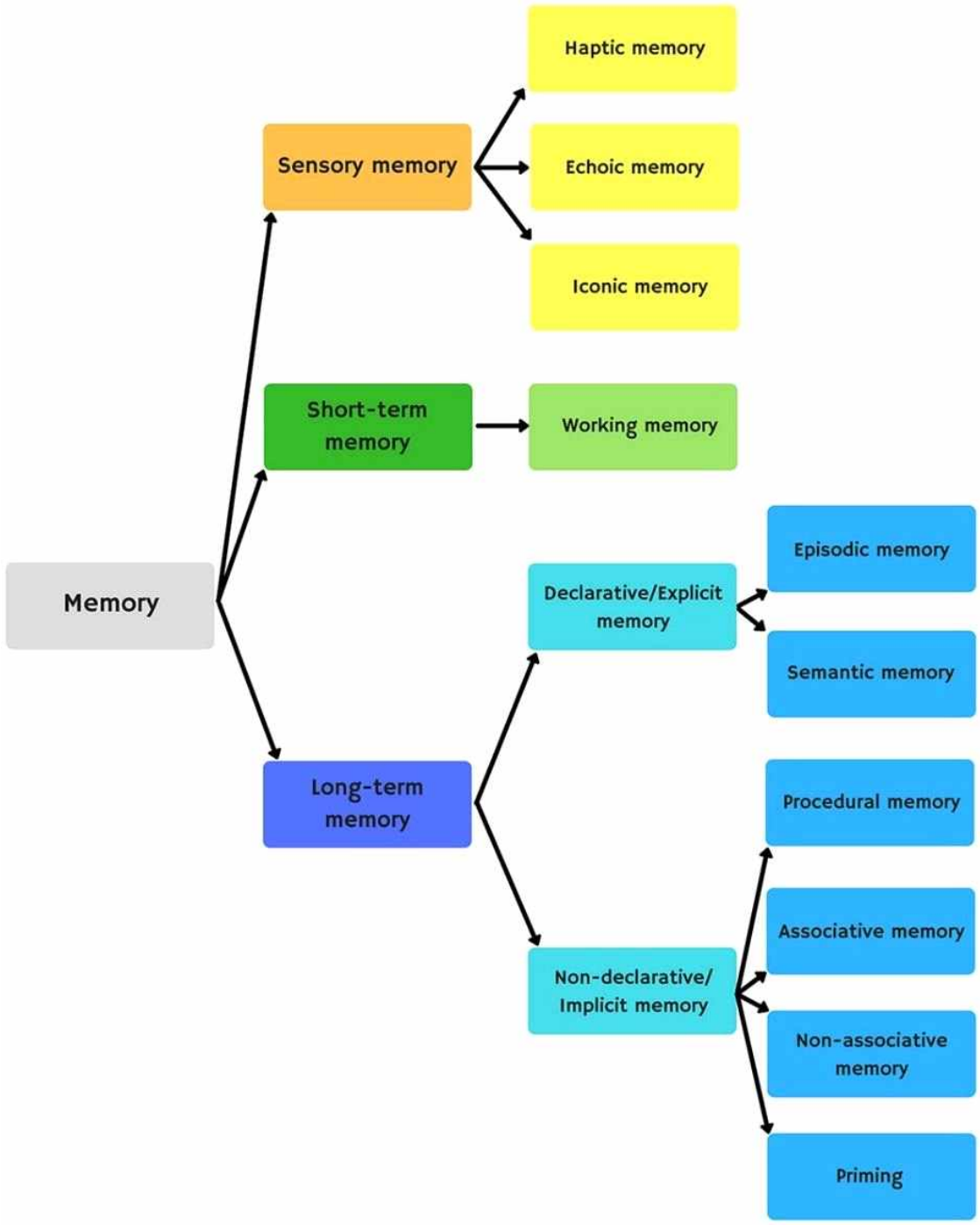

Figure 1.2 Memory classification. Sensory memory is formed by external sensory stimuli. Long-term memory is divided into declarative and non-declarative memory depending on the involvement of consciousness in memory recollection (Adapted from Camina & Guell, 2017).

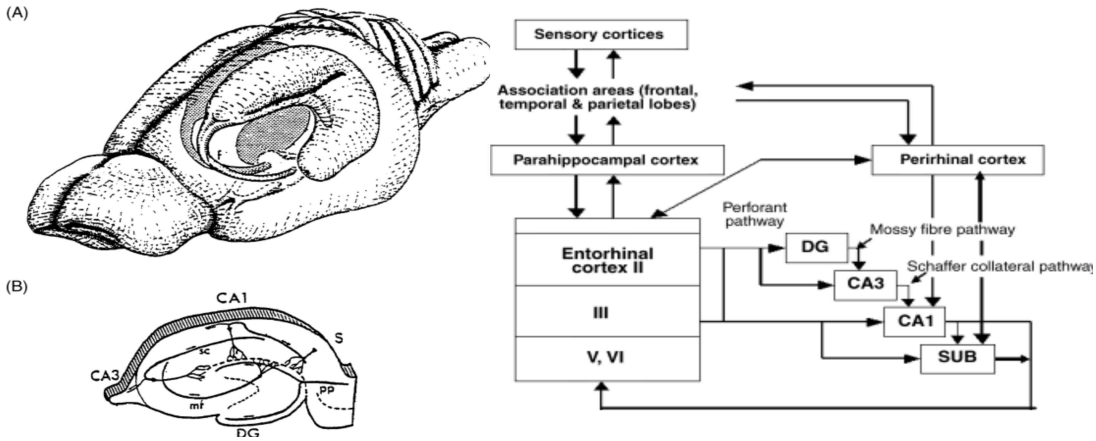

Figure 1.3. Hippocampal structure and internal connection in the hippocampal formation. (A) Hippocampus is an elongated C-shape structure under the cortical region. (B) Major hippocampal subfields and connecting fibers are shown in the slice of the hippocampus. DG: Dentate gyrus, CA1: cornu Ammonis 1, CA3: cornu Ammonis 3, S: Subiculum, mf: mossy fiber, pp: perforant pathway, sc: Schaffer collaterals. (C) Internal connection of hippocampus and parahippocampal circuitry. Sensory cortices project to the parahippocampal cortex and entorhinal cortex, a major source of input to the hippocampal proper. Projection to DG goes through CA3, CA1, and subiculum. Subiculum, a major output of the hippocampus, projects back to the parahippocampus, including the entorhinal cortex and perirhinal cortex. (Adapted from O' Mara, 2005).

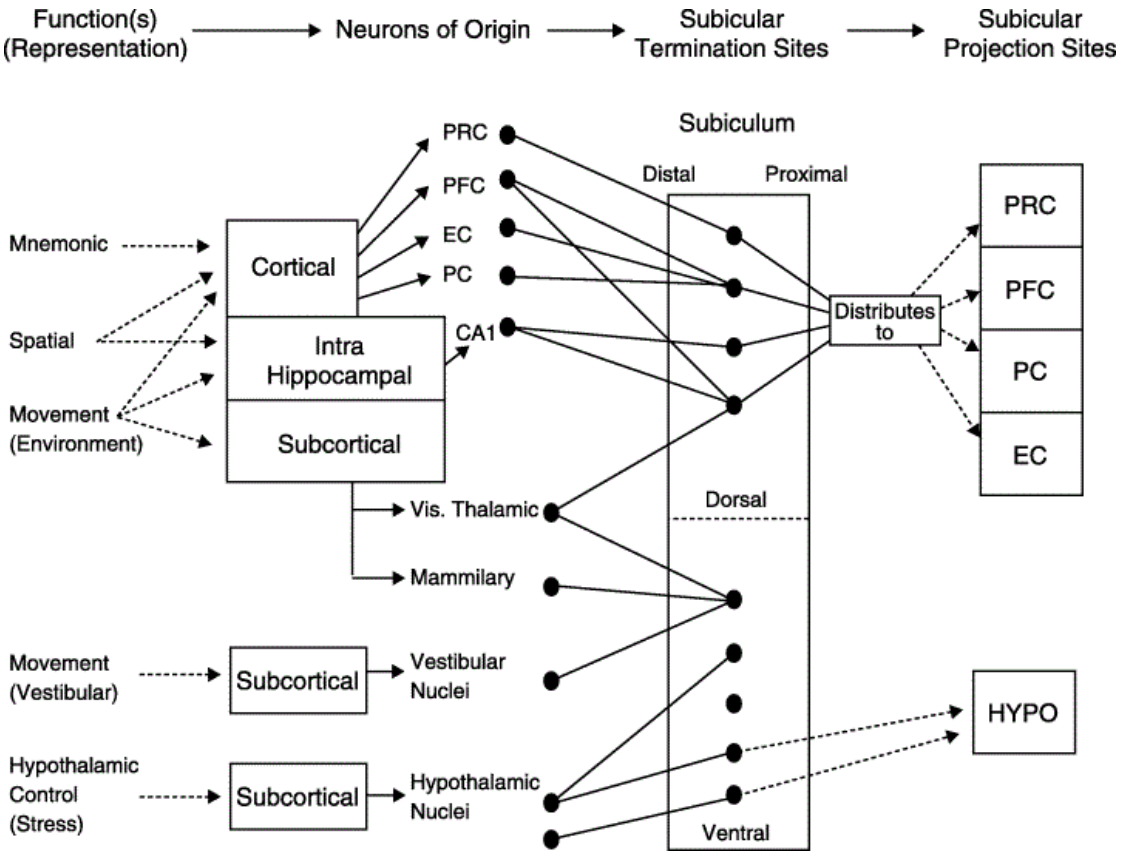

Figure 1.4: Input and output connection of subiculum, a main output of hippocampus. Different types of information are processed in various brain regions (cortex, hippocampus, subcortical structure) and projects to the subiculum. As a main output of the hippocampus, it abstract spatterns and projects different neuronal responses. EC: entorhinal cortex, Hypo: hypothalamus, PRC: perirhinal cortex, PFC: prefrontal cortex, PC: parietal cortex (Adapted from O' Mara, 2005).

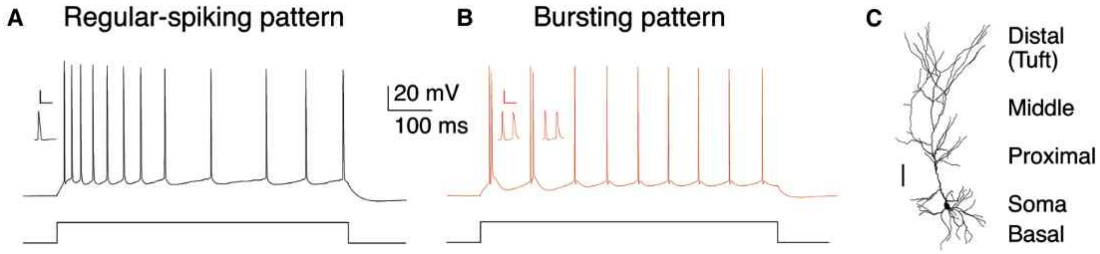

Figure 1.5. Firing pattern and morphology of hippocampal pyramidal neuron in CA1. (A, B) Pyramidal neurons responding to step current injection in vitro. Scale bar: 50mV and 20 ms. (A) A regular-spiking pattern of a pyramidal neuron consists of individual action potentials. (B) A bursting pattern of pyramidal neurons with one or more bursts of high-frequency spikes. (C) Pyramidal neurons with dendritic compartments (scale bar: 100nm) (Adapted from Graves et al., 2012).

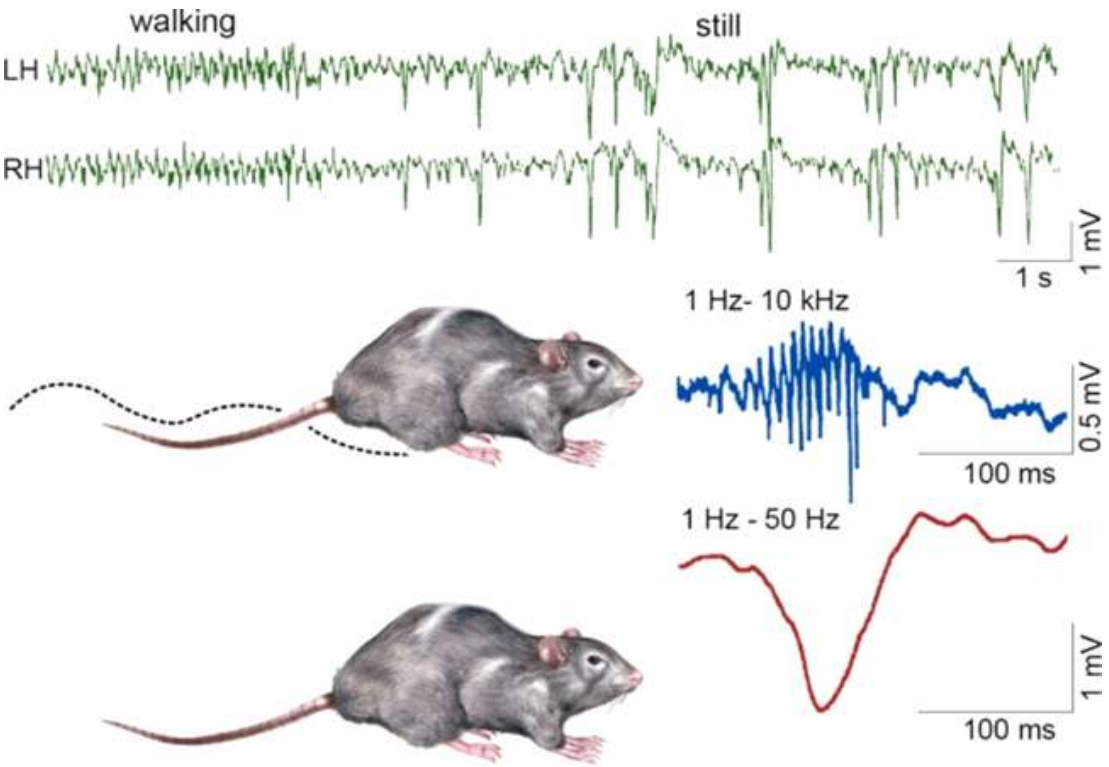

Figure 1.6 LFP signal recorded from left (LH) and right (RH) dorsal CA1. Bilateral synchronous negative waves (sharp wave) appear during still state. Red: Sharp wave, Blue: Ripples (Adapted from Buzsaki, 2015).

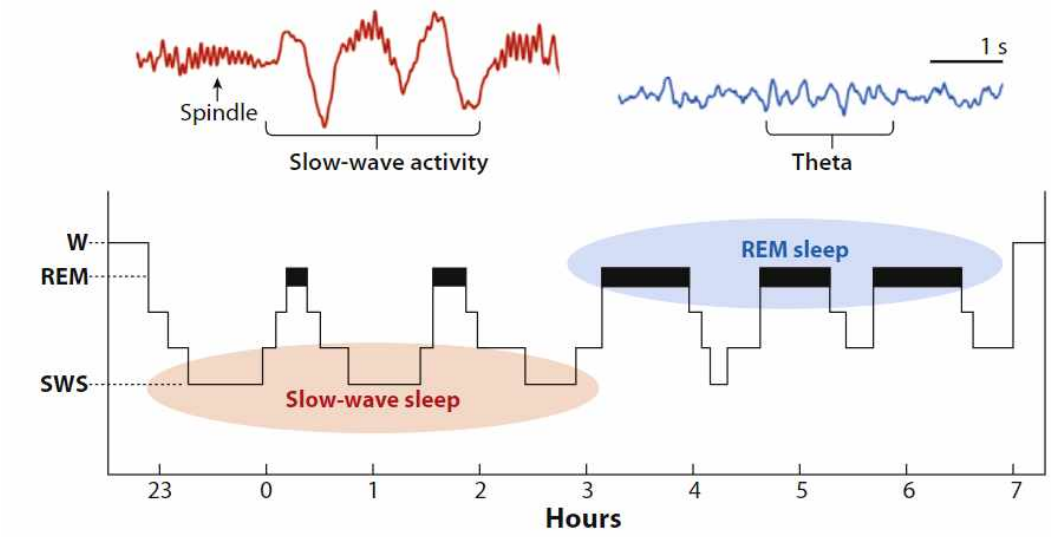

Figure 1.7. Sleep stage in humans. Sleep is divided into different stages, slow wave sleep (SWS) and rapid eye movement sleep (REM). SWS and REM alternate in cycle, and the first half of sleep is dominated by SWS and the latter half by REM sleep. Slow-oscillatory and spindle signals are hallmarks of SWS (Adapted from Vorster & Born, 2015).

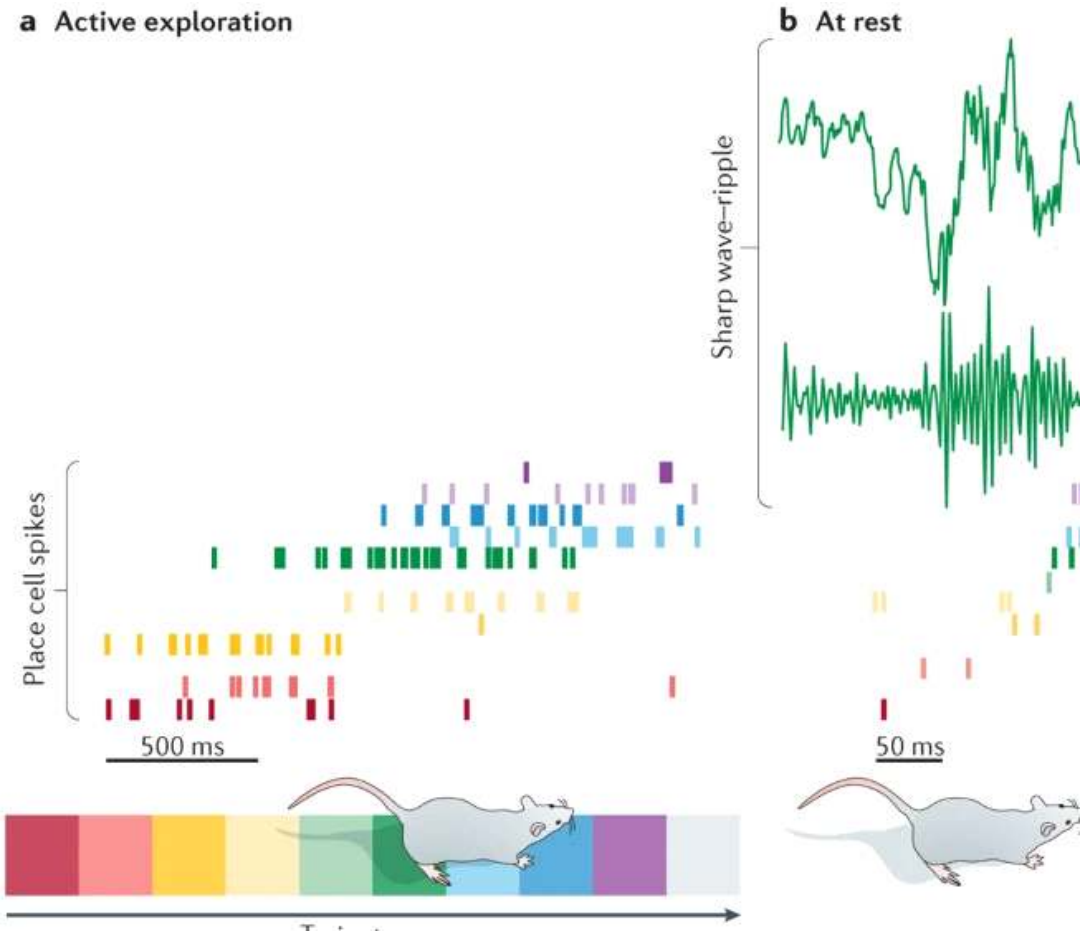

Figure 1.8: Hippocampal relay during sharp wave–ripple. A. Neuronal firing sequence of hippocampal place cells as an animal passes through place fields in a linear track. B. This firing pattern on the trajectory re–occur during post–experience phase. Replay appears with sharp wave–ripple signals (Signal in green, below) (Adapted from Colgin, 2016).

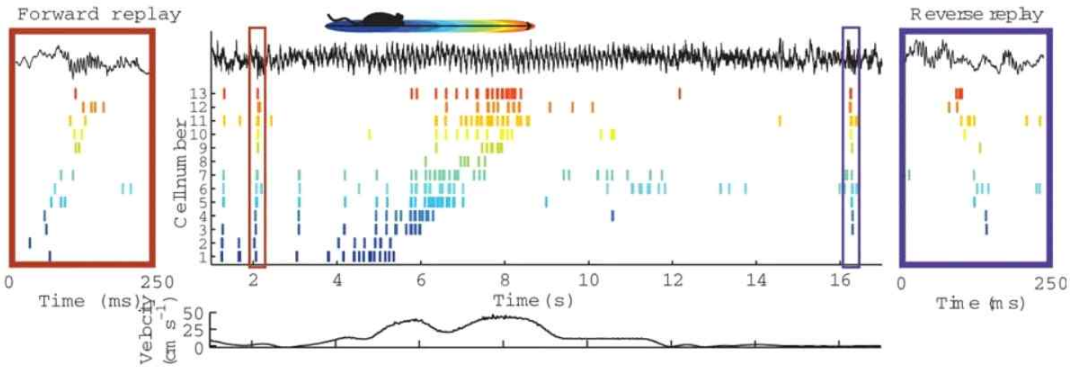

Figure 1.9. Forward and reverse replay of animal experience. Middle top: Spike trains from 13 place cells in CA1 of an animal running on the linear track. Middle bottom: velocity of the animal. During rest, hippocampal place cell fire with SWR in the LFP. Red box: neuronal spikes activated in sequence during rest (Forward replay). Blue box: neuronal spikes activated in a counter-sequence during rest (Reverse replay) (Adapted from Diba, K. & Buzsaki, G. 2007).

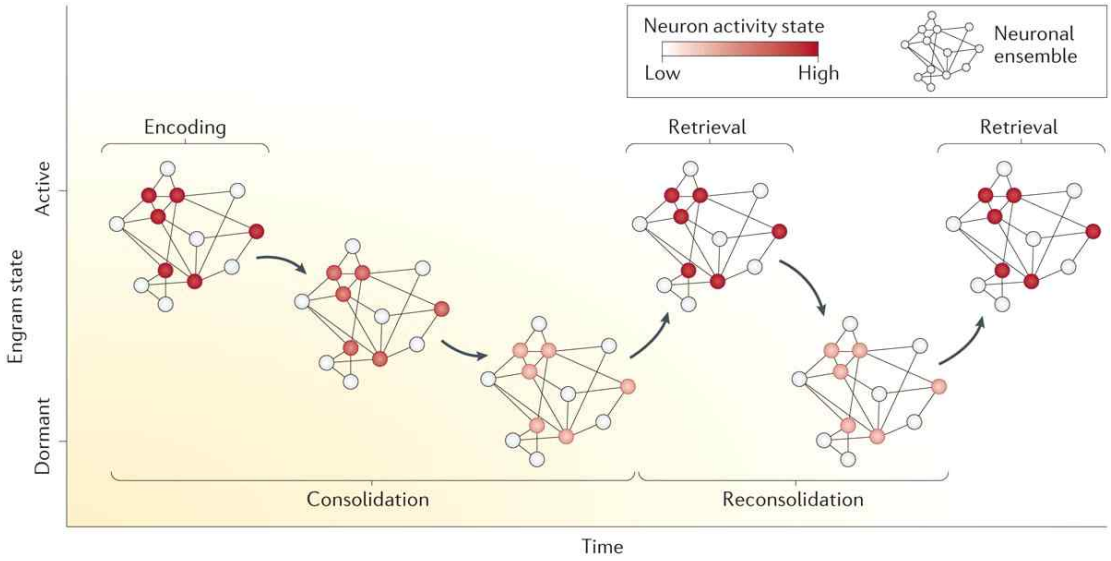

Figure 1.10. Memory process and engram. Among many neurons, subsets of neurons are active during events and encode information (memory encoding). The connection between encoded neurons is strengthened (consolidation) so that the same ensembles are likely to be reactivated together (retrieval). Engram is strengthened over time by repeated encoding and retrieval processes (Adapted from Josselyn et al., 2015).

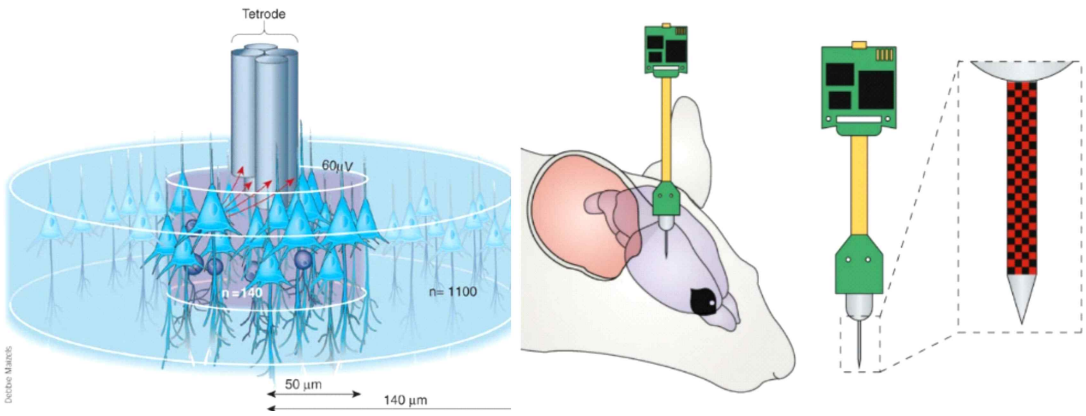

Figure 1.11: Electrophysiological recording using tetrode and silicon probes. (A) In the brain tissue, individual neuronal activities are recorded through 4 wires in tetrodes. From the recorded LFP, tetrodes estimate places of recorded neurons by the distance from each wire by triangulation (Adapted from Buzs□ki, 2004). (B) Silicon probe such as neuropixel probe has multiple recording sites integrated for stable recording and higher spatial resolution (Adapted from Hong & Lieber, 2019).

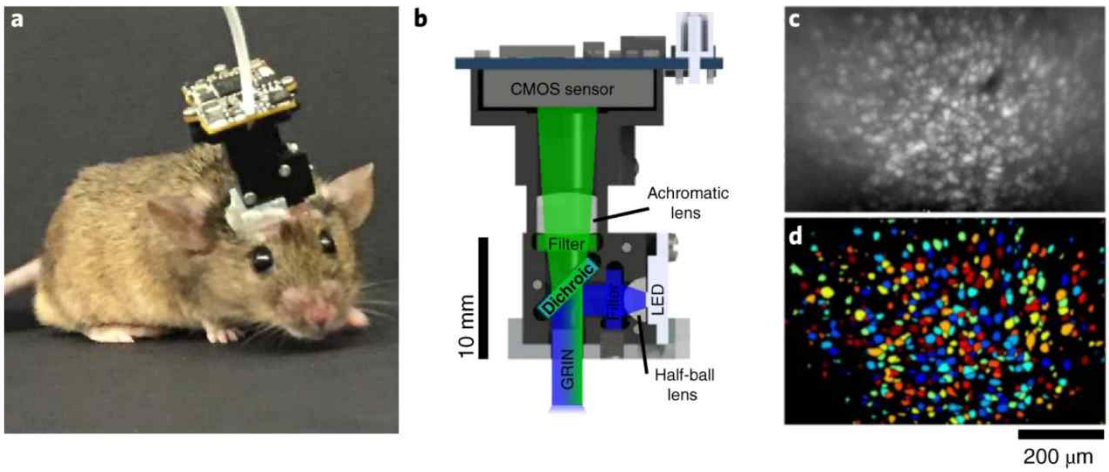

Figure 1.12: Miniaturized one-photon excitation microscope. A. UCLA Miniscope mounted on a mouse for in vivo recording. B. Internal structure of a miniaturized one-photon excitation microscope used in combination with GRIN lenses. When excitation LED emits a light source, it reflects on the dichroic mirror and excites brain tissue of interest. Emitted fluorescence from the tissue is transmitted to the CMOS sensor, the imaging detector. C Superimposed neurons recorded during 10mins from hippocampal CA1. D Spatial footprints of neurons from the recording in C. (Adapted from Aharoni et al., 2019)

Chapter 2. Simultaneous Cellular Imaging, Electrical Recording and Stimulation of Hippocampal Activity in Freely Behaving Mice

Summary

Hippocampal sharp wave-ripple activity (SWRs) and the associated replay of neural activity patterns are well-known for their role in memory consolidation. This activity has been studied using electrophysiological approaches, as high temporal resolution is required to recognize SWRs in the neuronal signals. However, it has been difficult to analyze the individual contribution of neurons to task-specific SWRs, because it is hard to track neurons across a long time with electrophysiological recording. In this study, we recorded local field potential (LFP) signals in the hippocampal CA1 of freely behaving mice and simultaneously imaged calcium signals in contralateral CA1 to leverage the advantages of both electrophysiological and imaging approaches. We manufactured a custom-designed microdrive array and targeted tetrodes to the left hippocampus CA1 for LFP recording and applied electrical stimulation in the ventral hippocampal commissure (VHC) for closed-loop disruption of SWRs. Neuronal population imaging in the right hippocampal CA1 was performed using a miniature fluorescent microscope (Miniscope) and a genetically encoded calcium indicator. As SWRs show highly synchronized bilateral occurrence, calcium signals of SWR-participating neurons could be identified and tracked in spontaneous or SWR-disrupted conditions. Using this approach, we identified a subpopulation of CA1 neurons showing synchronous calcium elevation to SWRs. Our results

showed that SWR-related calcium transients are more disrupted by electrical stimulation than non-SWR-related calcium transients, validating the capability of the system to detect and disrupt SWRs. Our dual recording method can be used to uncover the dynamic participation of individual neurons in SWRs and replay over extended time windows.

Introduction

In the field of systems neuroscience, uncovering communication between brain regions is one way of explaining their contribution to animal behavior, including learning and memory processes (Kandel, 2007). One widely used approach to tackle this question is the recording of neuronal activity from freely behaving animals using tetrodes or neural probes (Foster et al., 1989, Buzsaki et al., 2003, Buzsaki, 2015). Both measurements of single cell spiking activity and the local field potential (LFP) provide information about network computations. The high temporal resolution of these electrical signals enables the detailed study of neuronal synchronization and network dynamics that underly cognitive processes. While electrophysiological approaches are capable of recording from large populations of neurons, they suffer from difficulties to track cell identity long-term and offer limited information about the spatial organization and genetic identity of the cells.

Over the past years, single-photon Ca^{2+} imaging with miniature implantable microscopes has been established as an alternative method to measure cellular activity in freely behaving animals (Cai et al., 2016, Stamatakis et al., 2018, Scott et al., 2018, de Groot et al., 2020). In vivo chronic imaging not only keeps track of individual neurons across days but can also give detailed information about the spatial distribution of cells and whether they belong to genetically identified neuronal subpopulations. Some studies have used single-photon Ca^{2+} imaging in freely behaving animals successfully to elucidate the neuronal mechanisms underpinning specific behaviors (Cai et al., 2016, Stamatakis et al., 2018). However, because of the relatively slow dynamics of calcium transients, it is difficult to relate calcium signals to the specific timing of behavior and fast network dynamics. To better appreciate neuronal activity in freely moving animals in both temporal and spatial aspects,

it is necessary to complement Ca^{2+} imaging with electrophysiological recordings.

Sharp wave-ripple (SWR) is a characteristic neural activity pattern found in the hippocampus (Buzsaki, 2015, Buzsaki, 1989), showing highly synchronized bilateral occurrence in both adult and neonatal rodents (Benito et al., 2016, Fernandez-Ruiz et al., 2017, Shinohara et al., 2013, Suzuki & Smith, 1987, Hunt et al., 2018, Valeeva et al., 2019). The contribution of SWRs to memory, including memory consolidation (Milner et al., 1998, Alvarez & Squire, 1994, McClelland et al., 1995, Ramadan et al., 2009, Dupret et al., 2010), is widely studied in behavioral experiments using both correlation approaches and temporally-specific manipulations (Roux et al., 2017, Tang & Jadhav, 2019, Girardeau et al., 2009, Jadhav et al., 2012, Michon et al., 2019). The high-frequency (140-225Hz) SWR pattern in the hippocampus encodes behaviorally relevant cellular spike ensembles (Taxidis et al., 2015), suggesting its role in memory consolidation by re-activating previously activated neurons (replay) (Wilson & McNaughton, 1994, O' Neill et al., 2008, Gridchyn et al., 2020, Josselyn & Frankland, 2018). However, hippocampal replay has been studied mainly using electrophysiological approaches and it has been difficult to identify and track individual neurons that participate in a replay over time and across conditions. In addition, it has not been clarified how hippocampal neurons are affected by electrical stimulation used to disrupt SWRs in experiments that aim to test their role in behavior.

In this study, we combined electrophysiological recording and Ca^{2+} imaging simultaneously to investigate how cellular activity in the hippocampus changes during spontaneous and disrupted SWRs in freely behaving mice. We built a custom-designed microdrive and demonstrated simultaneous observation of SWRs from mice expressing the genetically encoded calcium sensor GCaMP6s.

We analyzed the cellular activity of hippocampal CA1 during spontaneous and disrupted SWR conditions acquired by both techniques. We observed significantly increased Ca^{2+} activity from hippocampal neurons surrounding spontaneous SWRs, but a silent signal in the SWR disrupted condition.

Materials and Methods

1. Animals

Animals were housed under standard conditions (12 h light: 12 h dark cycle) with food and water provided ad libitum. Data for this study were derived from a total of 4 Thy1-GCaMP6s-GP4.3 mice (2 males and 2 females, 10-16 weeks old) that were bred in-house. Robust expression of GCaMP6s in the hippocampus was confirmed in brain sections (Dana et al., 2014).

2. Design of implant

The implant consists of two components: a miniscope V3 (Labmaker, Germany) and a custom tetrode microdrive array. Taking advantage of the bilateral synchronous occurrence of SWRs (Buzsaki, 2015, Buzsaki, 1989, Valeeva et al., 2019), the microdrive array was devised to carry out electrophysiological tetrode recording from freely moving animals in the left hemisphere while the right hemisphere was imaged by the miniscope.

The microdrive array component was designed considering the anatomical position of three targets in the left hemisphere: dorsal CA1 (dCA1, for recording), the ventral hippocampal commissure (VHC, for stimulation), and white matter above the hippocampus (WM, for reference), using Allen Mouse Brain Explorer (http://mouse.brain-map.org/static/brainexplorer) as an

anatomical reference. SolidWorks (Dassault Systemes, France) was used for the 3D CAD design, and the microdrive array was printed using stereolithography (Formlabs, USA. Resin: photopolymer resin black (RS-F2-GPBK-04), gray (RS-F2-GPGR-04), or dental SG resin (RS-F2-DGOR-01). Printer model: Form 3).

The size and shape of the microdrive array were carefully designed to ensure enough surface for the implanted GRIN lens and the footprint of the miniscope. The main body (Figure 2.1 A, B) consists of three cannulas targeting the three brain regions (Figure 2.1 C). Each cannula guides a bundle of electrodes that is independently moveable through custom screws to control the insertion depth in the brain (Figure 2.1 B, arrow). The protective cover (Figure 2.1 D) still partially exposed the connector of the electrode interface board (EIB) and screw heads for convenient recording and tetrode adjustment during experiments without removing the cover (Figure 2.2 M).

3. Microdrive array fabrication

Multiple materials were required for building the tetrode microdrive (Figure 2.2 A), as follows:

a: 3D-printed protective cover, b: 3D-printed microdrive array body, c: electronic interface board (Neuralynx, USA), d: gold pins (Neuralynx), e: 2x M1.2 screws, f: a pair of female-male breakaway header pins (Farnell, UK), g: 2x ground wires (PFA-coated stainless steel wire, bare diameter: 127 μm, coated diameter: 203.2 μm, length: ~3cm; A-M system, USA), h: 1x self-tapping bone screw (shaft diameter: 1.19mm, length: 4.8mm; Fine Science Tools, Germany), i: 3x 23G tubing (Microgroup, USA), j: 3x custom-made microdrive screws (Kloosterman et al., 2009), k: 2x polyimide tubings (ID: 0.102mm, OD: 0.1397mm, length: ~50mm; Nordson, USA), l: 3x

30G tubings (length: ~55mm; Microgroup, USA), m: 3x 6mil pre-cut stainless-steel wires (length: ~80mm; Microgroup, USA) , n: 2x tetrode wires (four twisted 0.012 mm polyimide-insulated nickel-chrome wires, blunt cut; Sandvik, Sweden), o: 1x stimulus electrode (two twisted 0.06mm polyimide-insulated stainless steel wires, blunt cut; California Fine Wire, USA), p: thread-forming taps for M1.2 screws, q: tap handle, r: screwdriver, s: UV-curable dental cement (Dental elite, France). Detailed provider, model number, and costs of each material are provided in Table 2.1.

The detailed manufacturing steps are as follows (adapted from the previous protocol (Kloosterman et al., 2009, Nguyen et al., 2009)).

1) Tap and form thread for the five screw holes (arrows) in the microdrive body (Figure 2.2 A, b) using the thread forming tap (Figure 2.2 A, p). Use a tap handler (Figure 2.2 A, q) if necessary (Figure 2.2 B).

2) Prepare three screw-driven shuttles by connecting 23G tubing (Figure 2.2 A, i) and a microdrive screw (Figure 2.2 A, j) using UV-curable dental cement (Figure 2.2 A, s) using a mold (Figure 2.2 C).

3) Insert the shuttles into the microdrive body (Figure 2.2 D).

4) Insert the 30G tubing (Figure 2.2 A, l) into the 23g tubing of custom screws (Figure 2.2 E).

5) Cement the 30G tubings onto the outlet of cannulas in the microdrive array body using dental cement. On the outlet side, fill gaps between tubings and cannulas. On the opening side of the cannulas, make sure 30G tubing is positioned 2-3mm lower than 23G tubing (Figure 2.2 F).

6) Cut off excess 30G tubings from the outlet, and file the ends. Make sure 30G tubings have completely open ends by penetrating inserted 6mil wires (Figure 2.2 A, m). Remove wires after confirming a clear opening (Figure 2.2

G).

7) Prepare ground wires: solder one end of ground wire (Figure 2.2 A, g) to the female header pin (Figure 2.2 A, f, right) and connect the other end to EIB (Figure 2.2 A, c, arrow in Figure 2.2 H) using a gold pin (Figure 2.2 A, d). Solder one end of the other ground wire to the male header pin (Figure 2.2 A, f, left) and the other end to the stainless-steel screw (Figure 2.2 A, h). Cut the screw to 3-4mm and file the end (Figure 2.2 H).

8) Attach the EIB to the microdrive array body with screws (Figure 2.2 A, e). The ground wire goes through the hole in the bottom of the microdrive array (Figure 2.2 I).

9) Retract the custom screws to the level of the microdrive opening. The working distance of the screws is 7-8mm. Insert polyimide tubing (Figure 2.2 A, k) into 30G tubing. Cut excess polyimide tubing to the same length as 30G tubings (Figure 2.2 J). The polyamide tubing serves to guide and protect the tetrodes.

10) Prepare two tetrodes by twisting and heat-fusing four insulated electrode wires (Figure 2.2 A, n).

11) Insert tetrodes into the polyimide tubing. Insert a stimulus wire (Figure 2.2 A, o) into the third microdrive without polyimide tubing. Fix the stimulation electrode and tetrodes in the polyimide tubing using glue. (Figure 2.2 K).

12) After the glue has dried, secure tetrodes and the stimulus wire in the EIB using gold pins (Figure 2.2 L). Make sure tetrodes and stimulation wire have enough working distance of 7-8mm. Cut off excess wires.

13) Close the microdrive array with the 3D-printed cover (Figure 2.2 A, a). Fix the cover to the body using dental cement (Figure 2.2 M).

14) To lower tetrode impedance, goldplate tetrode tips (Nguyen et al., 2009)

1−4 hours before the implantation.

The total weight of the microdrive array is 2.2g, the height is 1.3mm, the largest width is 1.5mm, and the working distance of each custom−made screw in the cannula is approximately 7mm. A cross−section of the microdrive array is shown in Figure 2.1 B. The total weight that animals carry during experiments is 5.2g (microdrive array 2.2g + miniscope 3g, Figure 2.3 E).

4. Surgical procedure

For the simultaneous acquisition of calcium signal and LFP, animals underwent several surgical procedures including GRIN lens implantation, microdrive array implantation, and baseplating of the miniscope (Figure 2.3, A).

Gradient−index (GRIN) lens implantation

After induction of anesthesia (1.5% isoflurane in an induction chamber), the skull of the animal was securely fixed to the stereotaxic frame. Throughout the surgical process, the isoflurane level was maintained at 1−1.5% through a nose cap. The body temperature of the animal was monitored and kept at a constant temperature using a rectal probe and an electrical heating pad. After disinfection of the scalp with iodine and isopropyl alcohol, the skull was exposed. Craniotomy for the GRIN lens was made on the right hemisphere, a circle with the size of 0.95mm semi−diameter from the center (center coordinates: 4 mm posterior to bregma, 2.2 mm right from the midline). After exposing the brain in a circular shape, the dura, cortex, and white matter were gradually aspired until the hippocampus was exposed. GRIN lens (diameter: 1.8mm, length 4.31mm, Edmund Optics, UK) was inserted into the cavity of the brain at the speed of 50□m/10s. When the lens reached the target region,

the gap between the lens and skull was filled with Kwik-sil (WPI, USA) and then cemented to the skull by metabond (Parkell, USA)(Figure 2.3, B). The exposed GRIN lens was protected by a mass of Kwik-sil. Animals underwent 2 weeks recovery period after the implantation. CA1 under the implanted GRIN lens was imaged by miniscope to confirm the blood clearance and find image planes. If 20-30 cells were observed from the raw data, animals proceeded to the microdrive implantation.

Microdrive mounting

3 craniotomies were made to the skull to target 3 different brain regions (VHC: 0.0mm posterior to bregma, 0.2 mm right from the midline, Hippocampus: 1.1mm posterior to bregma, 1.5mm left from the midline, White matter and cortex: 4.1mm posterior to bregma, 1.5mm left from the midline). After the removal of dura from 3 craniotomies, the microdrive was mounted and cemented (Figure 2.3 C). A stainless screw with grounding wire was installed over the cerebellum and served as ground. Another end of the wire was carefully inserted into the sockets attached to the microdrive using breakaway header pins.

Miniscope baseplating

After 5-7 days of the postoperative period after microdrive implantation, we sought for imaging areas where the most calcium activities were found. Once the optimal imaging plane for long-term recording was chosen, a baseplate was mounted and cemented to the brain (Figure 2.3 D). After the baseplate was settled, miniscope sat on the baseplate and was adjusted to find the focal plane for imaging.

After all surgical processes were done, animals carried tetrode microdrive and baseplate in the cage (Figure 2.3 E), and miniscope was additionally mounted for experiments (Figure 2.3 F).

5. Electrophysiological recording

For the hippocampal SWRs recording and disruption, tetrode and stimulation wires were gradually lowered to the target brain regions. Electrophysiology was performed with the Digital Lynx 16SX (Neuralynx) data acquisition system with HS-18-LED analog headstage (Neuralynx) and Cheetah software (Neuralynx). Wide-band (0.1 Hz - 6 kHz) signals were sampled and digitized at 32 kHz. From the recorded tetrode signal, SWRs waveform was detected using a band-pass filter between 140Hz-225Hz. Multi-unit activity (MUA) was acquired by a band-pass filter between 600-6000Hz. The position of the animal was tracked and captured at 50 Hz using an overhead video camera using blue and red LEDs attached to the headstage. The location of tetrodes was confirmed by the presence of SWRs in the LFP.

6. In-vivo single-photon calcium imaging

After the microdrive array EIB was connected to the recording tether, the minicope was attached to the baseplate and firmly secured. Data acquisition was performed while animals performed unrewarded exploration in the open field (Figure 2.4 A) or a linear track (Figure 2.4 B). Image frames were acquired at 30Hz and timestamped in the DigiLynx acquisition system (Neuralynx) for synchronization with the electrophysiological signal (Figure 2.3 G, a). Time deviation between acquired image frames and theoretically generated frames was corrected by detecting missing frames and inserting

matching delays (Figure 2.3 K).

7. Online ripple detection and disruption

Digitized signals from the DigiLynx acquisition system were streamed to a workstation running the real-time processing software Falcon (Ciliberti & Kloosterman, 2017) (Figure 2.3 G, b). The signal was bandpass filtered in the ripple frequency band (135-225Hz) using a Chebyshev type-II IIR filter (order = 20). A ripple event was detected once the ripple power crossed a threshold that is computed from running estimates of the mean (μ) and mean absolute deviation (MAD) as μ + f x MAD. Here, f is a multiplication factor that was set manually to a value in the range between 9-14. For disruption, each ripple detection triggered a stimulator (A385 stimulus isolator, World Precision Instrument, USA) to produce a constant-current biphasic stimulation pulse (0.2 ms duration) in the ventral hippocampal commissure (Figure 2.3 G, c). The amplitude of the stimulation current was chosen such as to consistently disrupt hippocampal ripple events (range: 130μA and 20μA). The output stimulation frequency was limited to a maximum of 2Hz to avoid overstimulation. To avoid spurious detections induced by movement artifacts or stimulus-evoked responses, the above detection process was also applied to signals from the cortex overlying the hippocampus. Detections of hippocampal ripples that fall within a 1.5 ms- to 40 ms time window around spurious detections in the cortical signal were rejected.

8. 1-photon calcium imaging analysis

The acquired miniscope images were preprocessed semi-automatically with

the Python package Minian (https://github.com/DeniseCaiLab/minian). Briefly, the software subtracted the low-frequency background signal from the raw video and corrected for movement. The global baseline calcium signal was calculated, and ⊿F/F was computed for each video frame.

On the extracted ⊿F/F, spatial and temporal separation processes, and deconvolution of calcium transients were executed using the CNMF (Constrained Nonnegative Matrix Factorization) algorithm (Pnevmatikakis et al., 2016). In each step of the process, intermediate results of 10 randomly chosen cells were provided to guide manual intervention of the parameters for spatial and temporal distance for cell extraction. The final processed results included the spatial location of cells and calcium traces. Deconvolved calcium traces were binarized using GMM (Gaussian Mixture Model).

For each detected cell, an average of the lowest 30% of total signals in the spontaneous condition were used as a baseline in both conditions. Local maxima of the calcium signals higher than the baseline were detected and admitted as peaks. Considering the slow decay curve of the GCaMP6s (Chen et al., 2013), calcium peaks detected within 1s of online SWRs were classified as SWR-preceding peaks and the rest peaks were labeled as non SWR-preceding peaks.

9. Statistics

To compare the activity of cells during hippocampal SWRs to the activity without SWRs, we computed the average amplitude of peaks in each category of all units. The two-proportion z-test was used to compare the difference in proportions of unit properties in each category.

To compare the average peak amplitude ratio by peak properties, we

defined the ratio as a difference in peak amplitude of the two groups divided by the sum of the average peak amplitude of the two groups.

$$Peak\ amplitude\ ratio = \frac{sp - st}{sp + st}$$

sp: average peak amplitude in spontaneous condition

st: average peak amplitude in SWR-disrupted condition

A binomial test was used to examine the likelihood of the cell proportion above the chance level. Wilcoxon signed rank test was used to assess the effect of electrical disruption on SWR-related calcium activity for all units. 99% bootstrap confidence intervals were acquired by repeatedly computing medians from randomly detected samples 1000 times.

A two-sample t-test was used to compare average calcium traces between conditions. It was also used to compare the number of participating neurons at SWR events compared to random time points. The Kolmogorov-Smirnov test was used to compare the cumulative distribution of participating neurons for each SWR event or random time point.

10. Histology

After the experiments animals were deeply anesthetized (1.5% of isoflurane through a nose cap) and electrolytic lesions (constant current pulses, 60 μA, 20 seconds) were made to mark the location of the recording and stimulation electrodes. Animals were perfused with a phosphate-buffered saline solution followed by a 4% paraformaldehyde solution for fixation. The brain was stored in 30% sucrose solution, coronally sliced using a cryotome (Leica CM3050S,

thickness: 50㎛), and mounted on microscope slides. Brain sections were stained for Nissl substance and were covered using DPX (Sigma Aldrich) mounting medium. Brain sections were inspected under an optical microscope (Olympus MVX10) to examine the lesion marks and the GRIN lens insertion depth.

Results

Implant for combined cellular imaging, electrical recording, and stimulation

For the simultaneous acquisition of calcium and electrophysiological signals in hippocampal CA1 from freely behaving mice, we combined a miniscope for 1-P calcium imaging and a custom-made microdrive array for LFP recording. The microdrive array was designed using 3D-CAD software, 3D-printed, and was equipped with tetrodes and stimulation electrodes.

The miniscope endoscopic lens was implanted on top of the right hippocampal field CA1 (Figure 2.3 I). One tetrode was positioned near the CA1 cell layer in the left hemisphere to measure SWRs (Figure 2.3 J). The hippocampal calcium and electrophysiological signals from 4 freely behaving mice were acquired in two different recording conditions.

Simultaneous electrophysiological recording and 1-photon imaging from freely moving mice

4 animals explored a familiar arena (Figure 2.3 H, open field, 20 cm long sides) in a spontaneous condition.

Hippocampal LFP was characterized by theta oscillations as the animal was moving and SWRs as the animals paused. Fast and transient neural activity

patterns such as SWRs can be easily identified in the LFP (Figure 2.4 A).

Cellular calcium signals were acquired alongside the behavior and LFP (Figure 2.4 C left and right). We took advantage of the simultaneous imaging of cell activity and LFP recording to relate calcium signals to SWR events.

Hippocampal calcium imaging during SWR disruption by electrical stimulation

Using our dual recording system, we demonstrate the combination of electrical recording and disruption of SWRs together with the imaging of CA1 cell activity in freely behaving mice. Hippocampal LFP and calcium signals were collected while animals (n=4, 1 session per animal) stayed in the open field for 10 minutes (Table 2.2). Throughout the experiments, SWRs were detected online using a custom real-time processing system (Ciliberti & Kloosterman, 2017). For half the recording time (5 mins), SWRs were left unperturbed (Figure 2.4 A, left) and for the other half of the time (5 mins), SWRs were disrupted by a brief stimulation pulse in VHC (Figure 2.4 A, right). The order of spontaneous / SWR-disrupted condition blocks was randomized across recording sessions. We did not observe artifacts in the calcium images caused by electrical stimulation.

As shown previously (Michon et al., 2019), VHC stimulation evokes a short positive potential and reduces the ripple power in CA1 (Figure 2.4 B right), compared to the strong ripple power in the unperturbed signals (Figure 2.4 B left). Independently detected online SWRs were aligned to the analyzed calcium signals (Figure 2.4 C).

During the recording in the spontaneous or SWRs-disrupted condition, calcium transients of the detected neurons were recorded (Figure 2.5 A), and the signal was deconvolved to investigate neuronal spikes (Figure 2.5, B). SWR events were detected at the same time (Figure 2.5 A, B, top).

No difference in the peak property between SWR-related peaks and non-SWR-related peaks.

A total of 4976 detected calcium activities (Figure 2.6 A, purple dot) were detected during the whole recording period, and they were classified into two groups; 4487 peaks (90.17%) as SWR-related peaks and the rest (489 peaks, 9.83%, Figure 2.6 A, orange asterisk) as non-SWR related peaks.

To examine if there is a difference in the peak properties contributing to SWRs compared to non-SWR-related peaks, the event-triggered average of calcium peaks was calculated for the SWR-related group, and the activity was compared to the average of non-SWR-related groups as well as the average activity at the same number of random time points. The result showed that SWR-related peaks (Figure 2.6 B, blue) did not show a significant difference in the peak properties compared to non-SWR-related peaks (Figure 2.6 B, green, $p>0.05$, Two-sample t-test). When compared to the average of calcium transient collected at random time points, both SWR-related peaks ($p<0.0001$, Two-sample t-test) and non-SWR-related peaks ($p<0.0001$, Two-sample t-test) showed significant differences.

Effect of SWR-disruption on the calcium peak amplitude

We looked at the cell activity in the right CA1 as measured by calcium imaging (n=105, 122, 47, 46 cells in 4 animals). From all cells, all calcium peaks were classified into SWR-preceding peaks and non-SWR-preceding peaks depending on the presence of a preceding online-detected SWR within 2s. When comparing average amplitudes of peaks with preceding SWRs of all cells in the two conditions, most cells showed decreased amplitude in the SWR-disrupted condition than in the spontaneous condition (Figure 2.7 A).

This result implies an effective detection and disruption of SWRs, and our dual recording system confirms decreased calcium activity by the SWR disruption, especially when the peaks immediately follow SWRs. The effect of disruption was present in all animals (Figure 2.7 C). On the other hand, the proportion of unit properties based on the average peak amplitudes without preceding SWR signals in the two conditions showed that less proportion of units showed decreased peak amplitudes when the disruptive stimulation was applied ($p-value<0.0001$, Two proportion z-test, Figure 2.7 B). Also, the variation of proportion between animals was relatively larger (Figure 2.7 D).

Next, we compared the distribution of the average peak amplitudes of each peak group in the SWR-disrupted condition in relation to the spontaneous condition. The distribution showed that there is a significant difference between the two groups depending on the presence of preceding SWR. ($p-value<0.0001$, Wilcoxon signed-rank test, Figure 2.7 E).

Participating of neurons in each SWR event

Next, to investigate if more neurons are engaged at the SWR events than at other times, the number of participating neurons was counted for each SWR event and it was compared to the active neurons at the same number of random time points during the spontaneous condition (Figure 2.8 A). The distribution of SWRs by the number of participating neurons showed that more neurons are engaged at SWR events (mean: 34.66 neurons) compared to the same number of random time points (mean: 31.01 neurons) (Figure 2.8B, $p<0.0001$, Two-sample t-test). The cumulative distribution also showed that more neurons are active at SWR events compared to random time points (Figure 2.8 C, $p-value<0.0001$, Kolmogorov-Smirnov test).

While the result showed that more neurons synchronously fire at SWR events than at other time points, it remains elusive whether there are more dominating neurons contributing to SWR events than other neurons, or whether all neurons are equally participating in SWRs.

To distinguish differences in neuronal engagement in SWRs, the number of SWR events that each neuron participated in was counted. The result showed that each neuron has various participation rates, ranging from 1 to all events (Figure 2.9 A). Next, to understand the contribution power of each neuron to SWRs, the average SWRs power was calculated with (red) or without (gray) neurons (Figure 2.9 B). The result showed that there are some neurons contributing to the SWRs power more when the cells are engaged in SWRs, and these cells are categorized by differences in the SWRs power by their presence. The result showed that there are 3 cells showing more than 30% difference in average SWRs power depending on their presence (30%−group, Figure 2.9 A, B, red asterisks), 6 cells showing more than 20% difference in average SWRs power depending on their presence (20%−group, Figure 2.9 A, B, green asterisks), and 14 cells showing more than 10% difference in average SWRs power depending on their presence (10%−group, Figure 2.9 A, B, blue asterisks).

The influence of these neurons on the SWR events was examined by counting the number of events consisting of neurons in each group (Figure 2.9 C). The result showed that 3 cells in the 30%−group participated in 23 SWRs (6.66%, Figure 2.9 C, top), and 6 cells in the 20%−group participated in 104 SWRs (30.14%, Figure 2.9 C, middle). On the other hand, 14 cells in the 10%−group were found to participate in 325 SWRs, which cover almost all events (94.20%, Figure 2.9 C, bottom). These results show that there are a

few neurons that highly contribute to the power of SWR events than other neurons, and the higher the contribution is, the more selective their participation is in the events.

Discussion

In this study, we have presented a novel approach to combine tetrode recording, closed-loop stimulation and 1-photon imaging in freely moving mice. Electrophysiological recordings and cellular imaging complement each other to single out cells from aggregated signals, monitor target cells in the long term and have access to fast dynamics of neural activity.

Previous studies have combined single-photon microendoscope with deep brain stimulation (Trevathan et al., 2020) or silicon probe recordings (Zhou et al., 2019). To our knowledge, our study is the first to use a custom-designed implant for simultaneous electrophysiological recording, closed-loop electrical stimulation and single-photon microendoscope .

One of the critical requirements for the implant design is to secure enough space on the skull to implant the base plate of the miniscope. To reduce the volume of the microdrive array, we kept only the minimal components possible that make the drive functional. The thickness of the 3D-printed structures was minimized to reduce volume and weight while keeping robust stability for long-term recording. A shorter working distance of the microdrives would have reduced weight further, but we kept it at 7mm for future application in deeper brain areas. The microdrive array needs less than 8 hours manufacturing time, and we confirmed stable and fully functioning recording and stimulation for more than 5 months after implantation in some animals. This shows that our tool is suitable for long-term electrophysiological

recording and imaging from freely moving small animals with a short preparation time.

Hippocampal SWRs are well known for their role in memory encoding and consolidation during awake or resting states (Girardeau et al., 2009, Jadhav et al., 2012, Michon et al., 2019). Electrical stimulation applied to the VHC fibers is instantly transmitted to the hippocampus bilaterally, activating hippocampal principal neurons as well as interneurons. It triggers inhibition mediated by GABA receptor and increase of Ca2+−activated K+ conductance, and consequently, it silences the hippocampal network and immediately interferes with cellular activity (Girardeau et al., 2009, Ego-Stengel & Wilson, 2010). Disruption of SWRs by VHC stimulation has been used to study their contribution to learning (Ramadan et al., 2009, Michon et al., 2019, Ego-Stengel & Wilson, 2010). SWRs are ubiquitous and mostly occur synchronously in both hemispheres from the early stage of life (Buzsaki, 1989, Benito et al., 2016, Fernandez−Ruiz et al., 2017, Valeeva et al., 2019). We took advantage of this feature to enable measurements of the same SWRs by electrical recordings and CA^{2+} imaging in the left and right hippocampi respectively. According to our data, even though SWRs were detected in the left hippocampus, an increase in cellular calcium activity was also found in the right hippocampus. Likewise, disruption of SWRs by stimulation of the VHC also exhibited bilateral silencing of calcium activity in the hippocampus. Calcium activity that we observed is from a limited area of dorsal CA1, but as SWRs occur across an extensive region of the hippocampus, we assume that a substantial number of cells in the entire dorsal hippocampus are involved in this synchronized activity. It is generally hypothesized that hippocampal SWRs engage a wide cortical network that is required for rapid encoding of new information and the formation of long−term memory (Milner et al., 1998,

Alvarez & Squire, 1994, McClelland et al., 1995, Tang & Jadhav, 2019, Abadchi et al., 2020).

One of the mechanisms explaining the generation of SWRs is involved with triangular connections of pyramidal cells, PV+ basket cells, and other inhibitory populations. In the background state, pyramidal cells and PV+ basket cells fire at low rates, while inhibited by inhibitory populations (Csicsvari et al., 1999). When pyramidal cells excite PV+ basket cells, PV+ basket cells inhibit the inhibitory populations which consequently disinhibit the pyramidal cells (Chenkov, 2017, Evangelista et al., 2020). Accordingly, disinhibited pyramidal cells and PV+ basket cells start to fire at high frequencies while inhibitory neurons stay silent, and the balance of activities is maintained during SWRs (Klausberger et al., 2003, Varga et al., 2012). When the high firing rate of PV+ basket cells leads to short-term depression of their efferent synapses to the inhibitory population (Kraushaar & Jonas, 2000, Kohus et al., 2016), SWR is terminated by inhibition of pyramidal cells (Chenkov, 2017, Evangelista et al., 2020). Although interneurons are involved in the generation of SWRs, their activities seem to be less pronounced in this study because both electrophysiological and calcium imaging approaches are conducted on the cellular layer of the hippocampal CA1.

From our result, it was observed that more neurons fire at each time point of SWR events compared to random time points, while the peak property was not different either at SWR time points or at other times. Considering that the immediate and concurrent firing of pyramidal neurons and PV+ basket cells are the source of ripple signals, it is assumed that the synchronous firing of numerous neurons might be more critical for the onset of SWR events, rather than particular features of the peak property.

There are some limitations to our approach. First, even though there is

broad literature about the synchronous occurrence of SWR in both hippocampi, there is also indication that SWRs in both hemispheres may have different timing (Villette et al., 2017). Such (partial) inter-hemispheric decorrelation would have resulted in an underestimate of the calcium response to SWRs in our data. Second, for online SWR detection there is a 20-30 ms delay between the onset of SWR and electrical stimulation. Therefore, when disrupting SWRs, the initial part of each SWR is still intact. Even so, we did not find any evidence of SWR-related calcium response following electrical disruption. Lastly, we classified calcium peaks into two groups depending on the presence or absence of SWRs within the preceding 2s of each peak, considering the slow temporal dynamics of GCaMP6s. Future studies would benefit from the use of calcium indicators with faster dynamics to reveal the timing relation between SWRs and subsequent calcium response in more detail.

In summary, our study presented a new custom-designed microdrive and its application in recording hippocampal activity. We implanted the microdrive in the hippocampus and investigated calcium activity patterns in two different environments from freely behaving animals. Also, we compared calcium activity during intact and disrupted SWRs, which suggests extensive and synchronous participation of neurons during SWR activity. With further analysis, our data can potentially reveal individual cells and cellular ensembles that participate in SWRs, spatial/temporal connections of neurons, and their change over time to coordinate memory processing. Identifying cellular patterns would enable cell- or ensemble-specific SWR disruption to uncover the detailed mechanism of memory formation. Last but not least, although we introduced the application of our microdrive by recording and disrupting hippocampal activity, it can also be adopted to other brain regions with modification of design and implant location.

Material availability

3D printing files and custom python code used in this study is available at https://bitbucket.org/kloostermannerflab/combined-microdrive-and-miniscope/

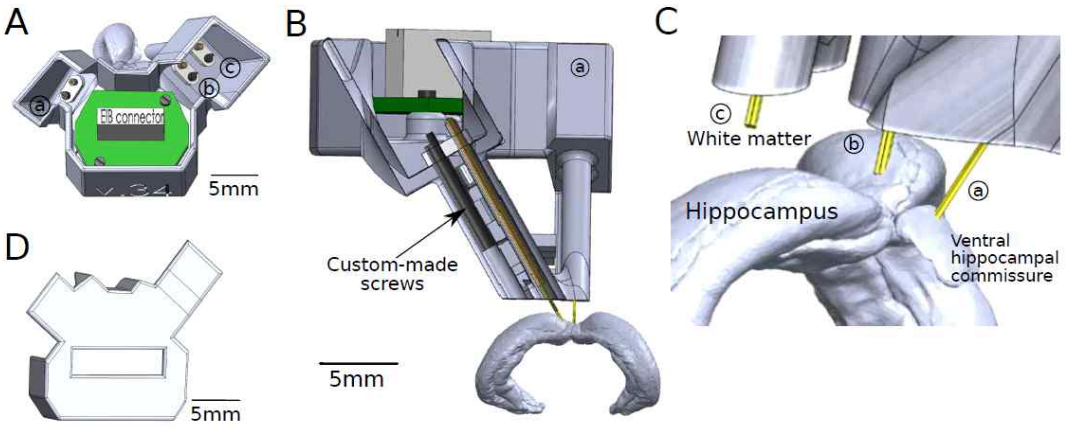

Figure 2.1. Design and structure of the microdrive (A) Top view of a 3D CAD model of the microdrive with electrical interface board (EIB). a Screw-driven shuttle for stimulation electrode targeting VHC. b Screw-driven shuttle for tetrode targeting hippocampus CA1. c: Tetrode in the white matter for reference purposes. (B) Cross-section of one of the microdrive cannulas. The insertion depth of the stimulation electrode and tetrodes (yellow) were controlled by custom screws (black, arrow). (C Close-up view of tetrodes emanating from the microdrive array and their target areas. (D) Cover of the drive for the protection of electrical components.

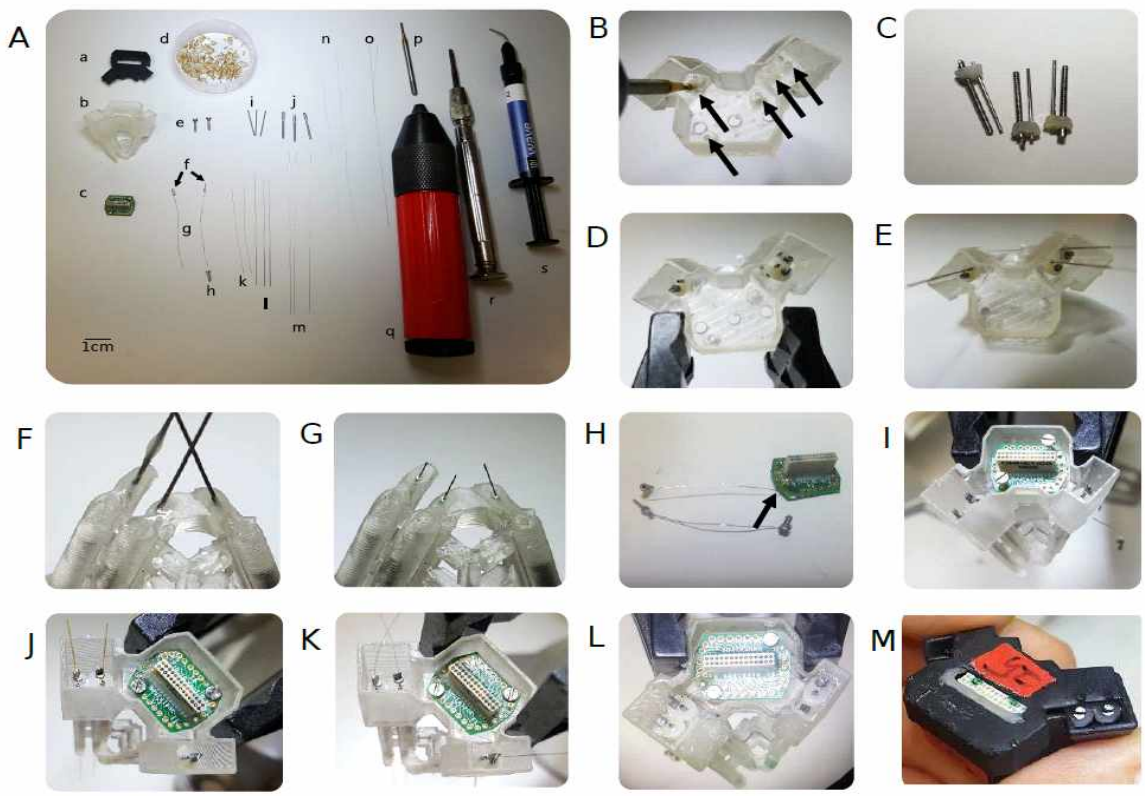

Figure 2.2. Microdrive array fabrication materials and process. (A) Microdrive materials. Detailed list with providers is in the method section (2.3). (B–M Microdrive array fabrication procedure. Detailed explanation is in the method section (2.3).

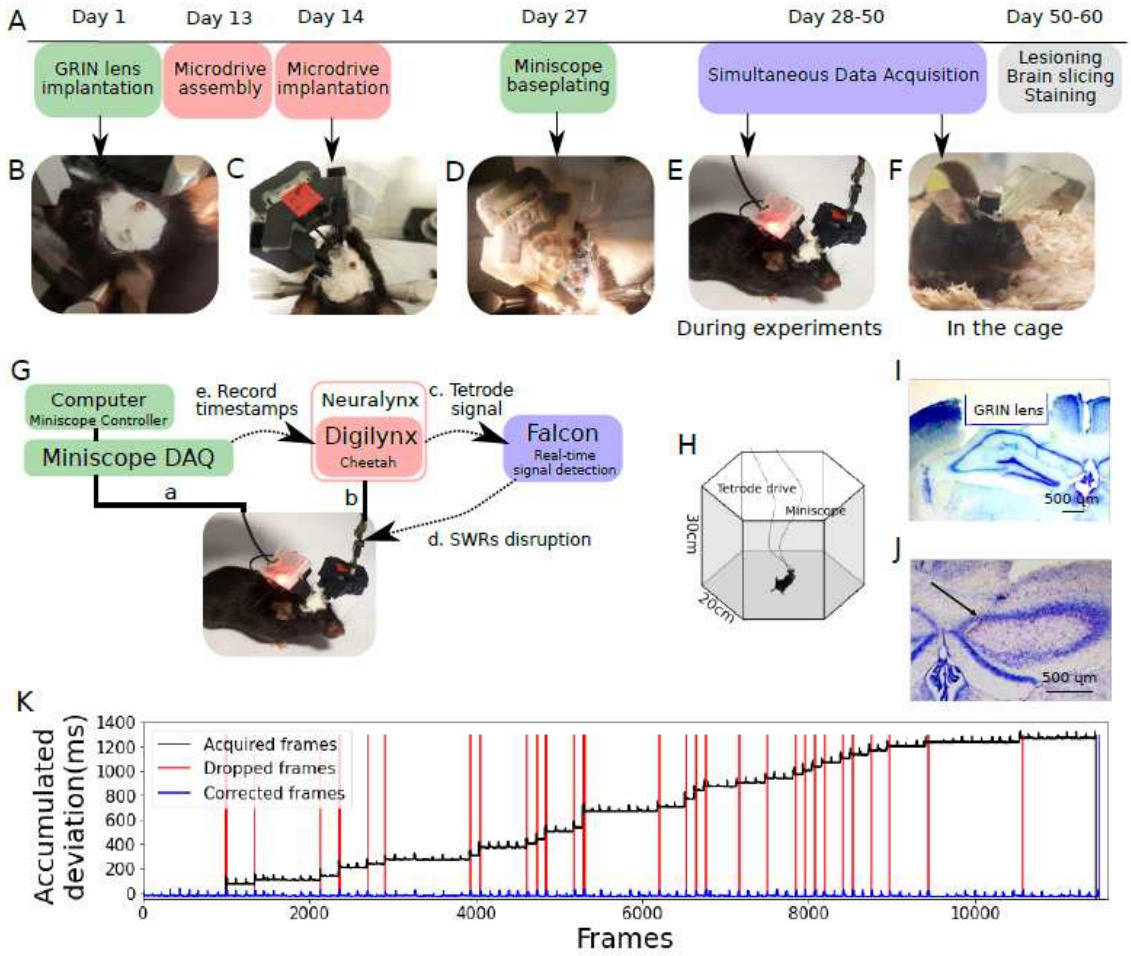
A
Day 1
Day 13
Day 14
Day 27
Day 28-50
Day 50-60
GRIN lens implantation
Microdrive assembly
Microdrive implantation
Miniscope baseplating
Simultaneous Data Acquisition
Lesioning Brain slicing Staining
B
C
D
E
F
During experiments
In the cage
G
Computer
Miniscope Controller
Miniscope DAQ
e. Record timestamps
Neuralynx
Digilynx
Cheetah
c. Tetrode signal
Falcon
Real-time signal detection
a
b
d. SWRs disruption
H
Tetrode drive
Miniscope
30cm
20cm
I
GRIN lens
500 µm
J
500 µm
K
Accumulated deviation(ms)
Acquired frames
Dropped frames
Corrected frames
Frames

Figure 2.3. Experimental timeline and recording system. (A) Experimental timeline. Single-photon calcium imaging: GRIN lens was implanted on the surface of the hippocampal CA1 of the right hemisphere (Day 1), and blood clearance at the surgical site was confirmed 2-3 weeks after the implantation (B). When calcium activity was observed through the implanted lens, mice were equipped with a baseplate (Day 27) to mount the miniscope (D). Once microdrive implantation was consolidated, miniscope was mounted on the baseplate and data acquisition was performed simultaneously with the LFP recording (Day 28-50) (E). lectrophysiological recording: Microdrive array manufacturing takes 1 day (8 hours, Day 13). Assembled microdrive array was carefully implanted above the target brain regions (Day 14) (C). After implantation, animals underwent 5-7days of post-operative recovery. After recovery, electrophysiological signals were acquired, together with the calcium signal (Day 28-50) (E). In the home cage animals only carried the microdrive array, but not the miniscope, which was mounted onto the baseplate just prior to the start of the recording session. After experiments were completed, the implantation sites for the GRIN lens and tetrodes were validated histologically (Day 50-60) (F). (G) Set up of the acquisition system for simultaneous imaging, electrical recording, and closed-loop stimulation. 1-photon calcium signal was acquired by miniscope connected to a dedicated computer using Miniscope Controller software (a). Electrical signals were acquired with a Digilynx acquisition system and stored on a computer running Cheetah software (b). The digitized electrical signals were also streamed to a separate computer running Falcon software for real-time hippocampal ripple detection (c) and closed-loop feedback stimulation in the VHC (d). Each video frame from the miniscope was timestamped in the Digilynx system for synchronization with the electrical signals (e). (H) Recording chamber. (I) Coronal section of the dorsal hippocampus showing the location of the implanted GRIN lens. (J) Coronal section of the dorsal hippocampus showing a tetrode track. The arrow indicates the lesion made by an electrical current applied to the tetrode to verify the recording location. (K) Accumulated time deviation between acquired frames and theoretically generated frames of calcium imaging (Black: acquired frames, Red: timepoint of dropped frames, Blue: Corrected frames).

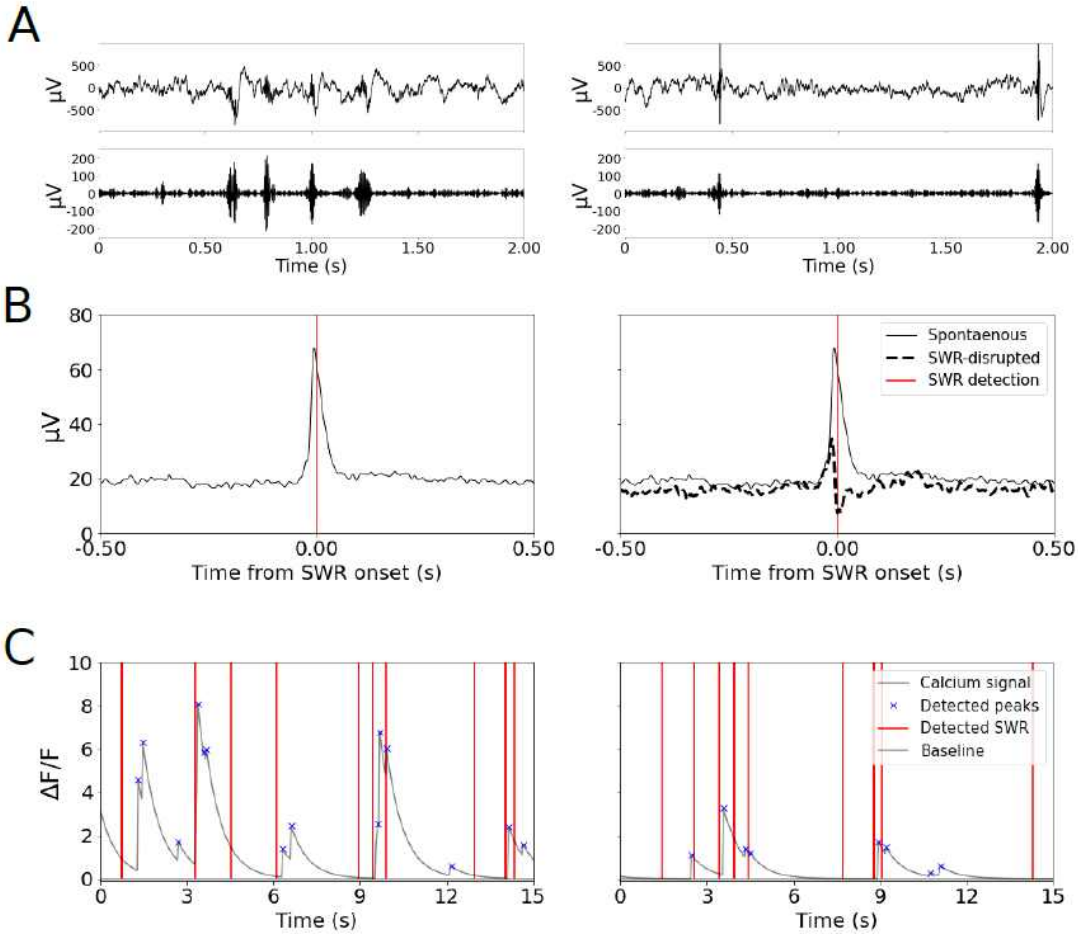

Figure 2.4. Electrophysiological signals and calcium transient were simultaneously acquired in spontaneous and SWR-disrupted conditions from freely behaving animals. All data from one representative animal (Animal 1) SP: average peak amplitude in spontaneous condition, ST: average peak amplitude in SWR-disrupted condition. (A) Representative wide-band filtered (1-6000Hz, top) and ripple-band filtered (140-225Hz, bottom) hippocampal LFP signal in the spontaneous condition (left) and SWR-disrupted condition (right). (B) Average spontaneous SWR power (left) and disrupted SWR power (right, dashed) (red: SWR detection). (C) Representative calcium signals in the spontaneous condition (left) and SWR-disrupted condition (right) (red: SWR detection, blue: detected peaks, gray: baseline).

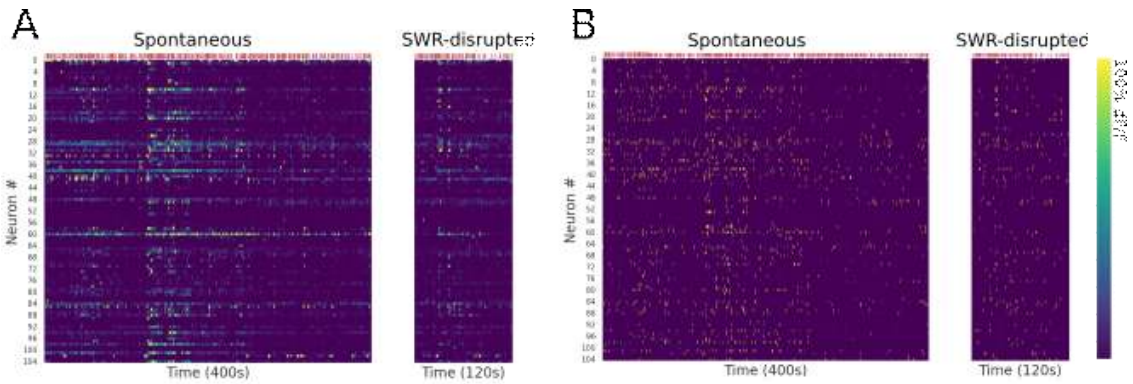

Figure 2.5. Representative calcium and deconvolved calcium activity recorded from the hippocampus during spontaneous and SWR-disrupted conditions of one session. (A) Left: SWR onset detection (Top, red) and color raster of the fluorescence signal (dF/F) of calcium transient in the spontaneous condition (Bottom). Right: SWR onset detection (Top, red) and color raster of the fluorescence signal (dF/F) of calcium transient in the SWR-disrupted condition (Bottom). (B) Left: SWR onset detection (Top, red) and color raster of the fluorescence signal (dF/F) of deconvolved calcium transient in the spontaneous condition (Bottom). Right: SWR onset detection (Top, red and color raster of the fluorescence signal (dF/F) of deconvolved calcium transient in the SWR-disrupted condition (Bottom).

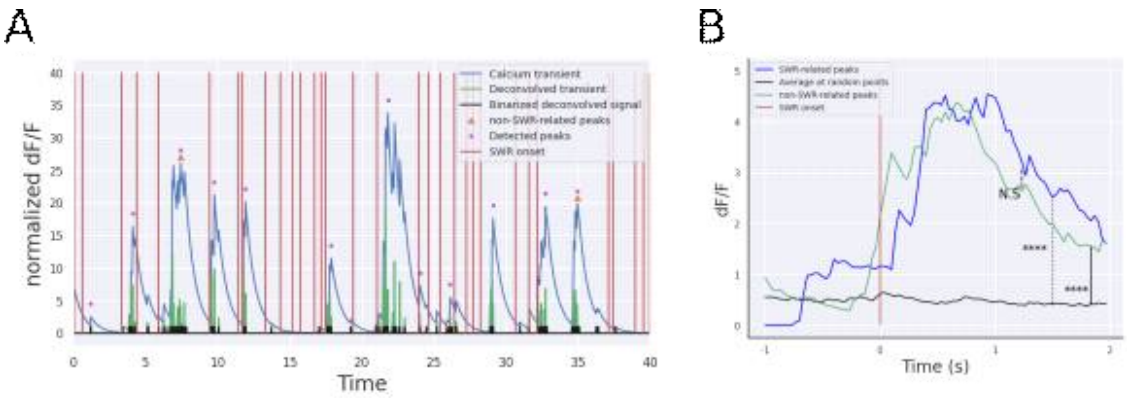

Figure 2.6. The average calcium peak property at SWR events is not significantly different from average non-SWR-related calcium peaks. (A Representative raw traces of recorded signal in the spontaneous condition (Blue: calcium transients, green: deconvolved calcium signal, black: binarized deconvolved calcium signal, red: detected SWR events, purple dot: detected peaks, orange triangle: non-SWR-related peaks). (B) Blue: Average SWR-related calcium peaks (Blue). Green: Average of non-SWR-related calcium peaks (Green). Average calcium transient at random time points (Black) (Dashed: SWR-related peaks vs non-SWR-related peaks, N.S p-value=0.36. Dotted: SWR-related peaks vs average transients at random time points, p-value=2.72e-20. Solid: non-SWR-related peaks vs average transients at random time points, p-value=9.56e-20. Two-sample t-test were applied to compare averages).

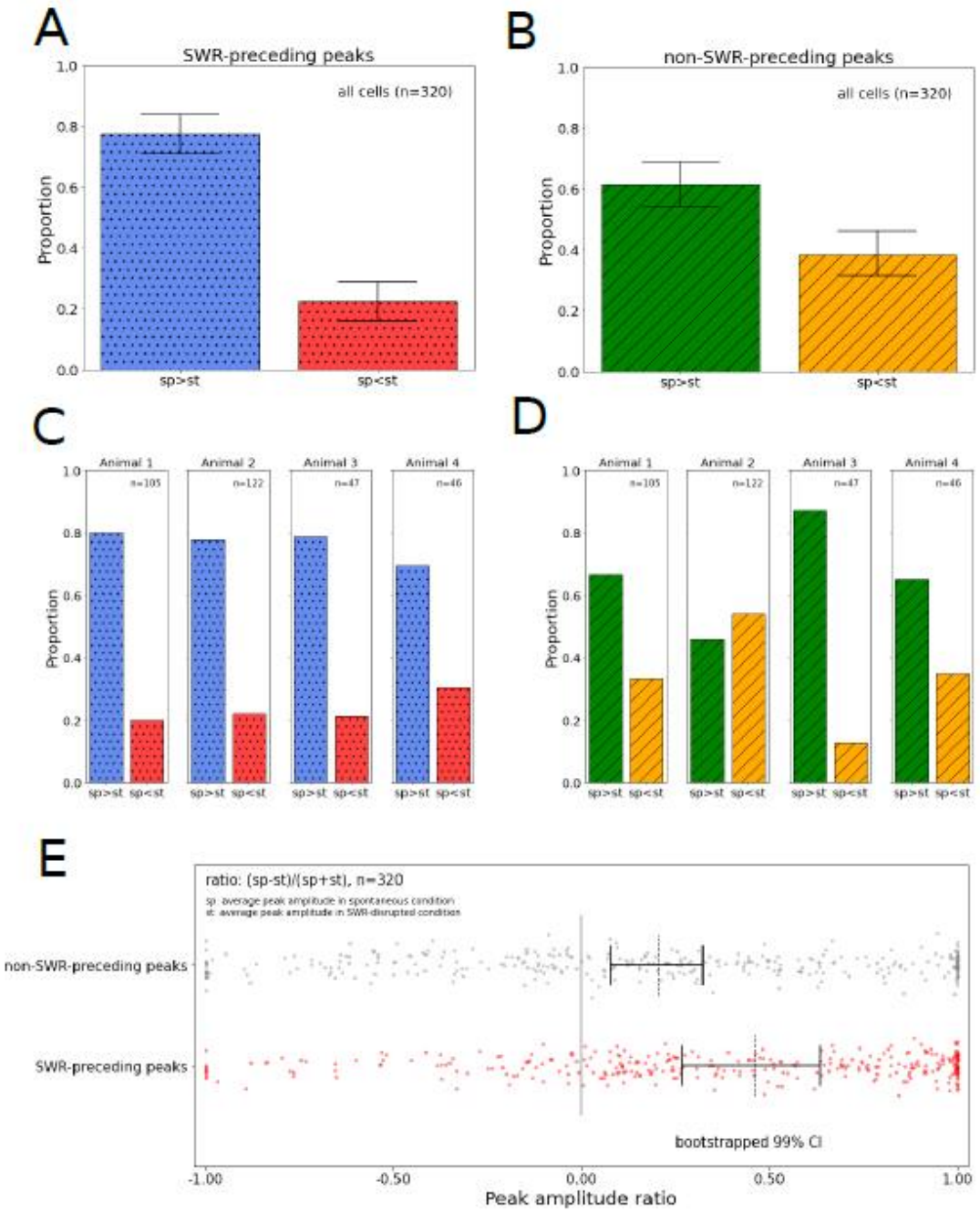
A
SWR-preceding peaks
all cells (n=320)
Proportion
sp>st
sp<st
B
non-SWR-preceding peaks
all cells (n=320)
C
Animal 1
Animal 2
Animal 3
Animal 4
n=105
n=122
n=47
n=46
D
E
ratio: (sp-st)/(sp+st), n=320
sp: average peak amplitude in spontaneous condition
st: average peak amplitude in SWR-disrupted condition
non-SWR-preceding peaks
SWR-preceding peaks
bootstrapped 99% CI
-1.00
-0.50
0.00
0.50
1.00
Peak amplitude ratio

Figure 2.7. Different subsets of cells respond to SWRs depending on the behavioral state. Calcium peaks from all cells were classified into two categories depending on the presence of preceding SWRs. (A, C): SWR-preceding peaks, (B, D): non SWR-preceding peaks. (A) Proportion of units by the SWR-preceding peak property from all units. Left: proportion of units where the peak amplitude decreased in the SWR-disrupted condition. Right: proportion of units where the peak amplitude increased in the SWR-disrupted condition. (Total units: 320, p-value=4.26e-24, solid: bootstrapped 99% confidence interval) (B) Proportion of units by the non SWR-preceding peak property from all units. Left: proportion of cells for which the peak amplitude decreased in the SWR-disrupted condition. Right: proportion of units where the peak amplitude increased in the SWR-disrupted condition. Proportions of Figure 2.5A and Figure 2.5C were statistically compared using a two proportion z-test (p-value<0.001). (Total units: 320, p-value=2.08e-05, solid: bootstrapped 99% confidence interval). (C) Proportion of units by the SWR-preceding peak property from individual animals (Animal 1: 105 units, animal 2: 122 units, animal 3: 47 units, animal 4: 46 units). (D) Proportion of units by the non SWR-preceding peak property from individual animals (Animal 1: 105 units, animal 2: 122 units, animal 3: 47 units, animal 4: 46 units). (E) Distribution of average calcium peak amplitude ratio of SWR-disrupted condition compared to the spontaneous condition of peaks with preceding SWRs (red) and peaks without preceding SWRs (gray) of 90% of units during the whole recording (Wilcoxon rank-sum test, p<0.0001, dashed: median, solid: bootstrapped 99% confidence interval. The gray line indicates where the average calcium peak amplitude in the spontaneous condition is equal to the average calcium peak amplitude in the SWR-disrupted condition).

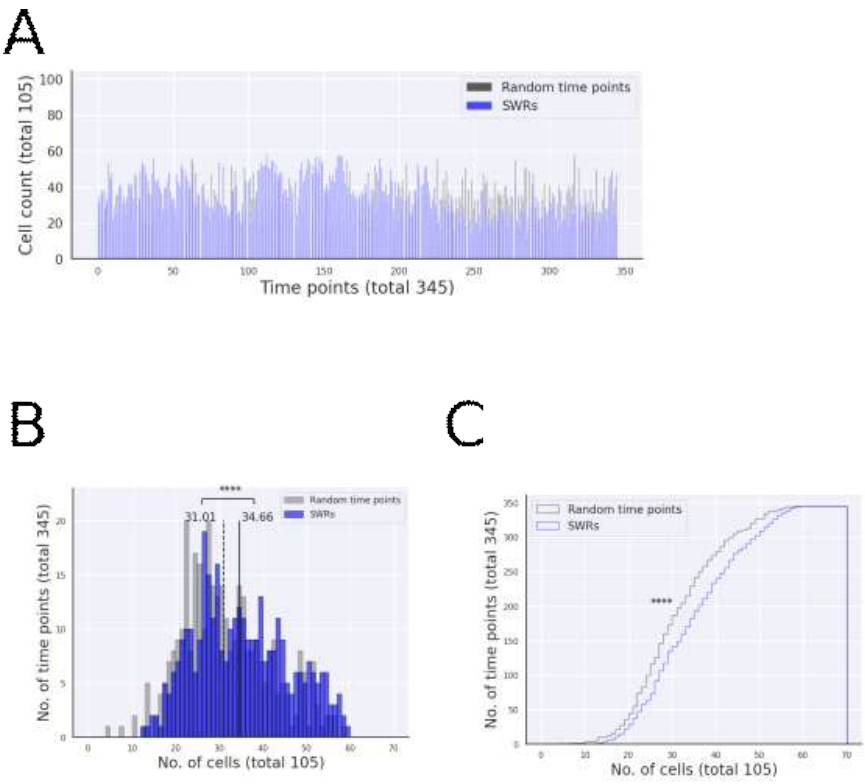

Figure 2.8. More neurons are engaged at SWR events compared to random time points. (A) Number of participating neurons for each SWR event time point (blue) compared to random time points (gray). (B) Distribution of SWR events (blue) and random time points (gray) by the number of active neurons for each event. The distribution of the number of neurons participating in each SWR event (average 34.66, solid) is significantly different from the number of neurons active at random time points (average 31.01, dashed) p-value=6.40e-06, Two sample t-test). (C) The cumulative distribution of the number of events (blue: SWR events, gray: random time points) by the participating neurons for each time point (p-value=8.01e-05, Kolmogorov-Smirnov test).

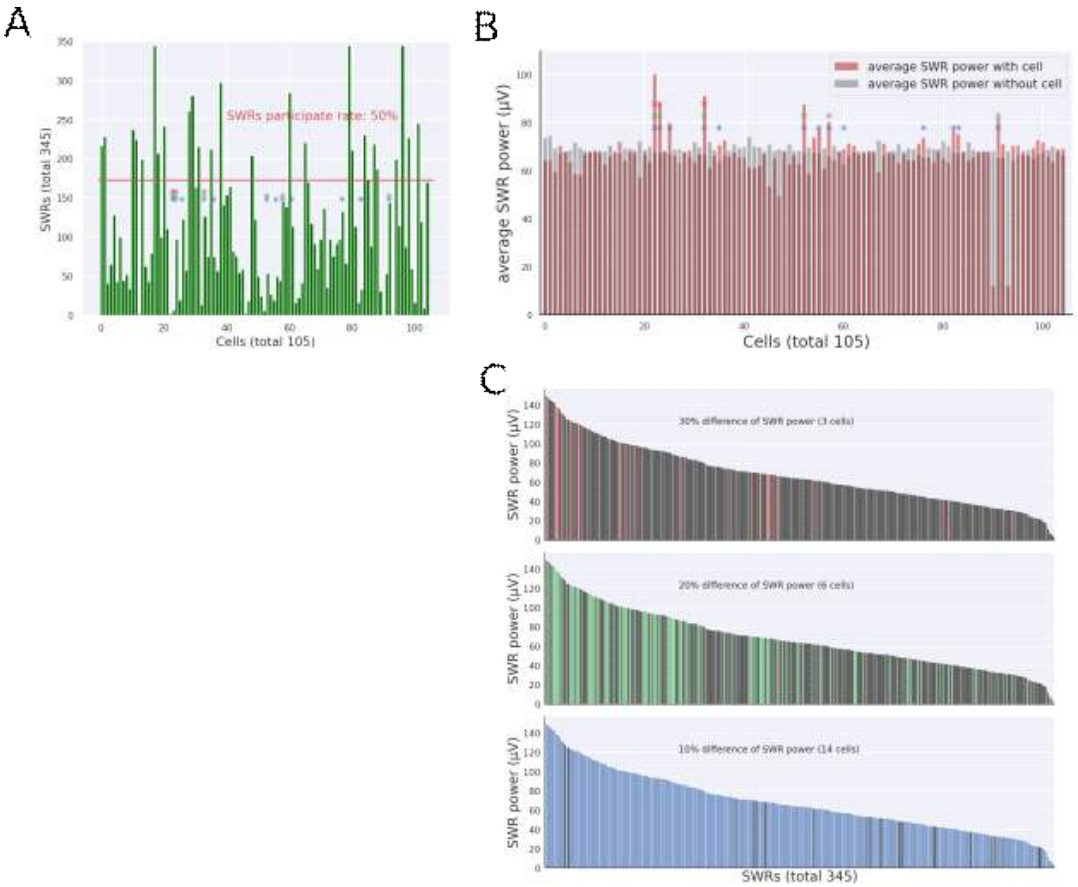

Figure 2.9. Participation of neurons at each SWR event. (A) Number of SWR events participated by each neuron. (Red line: 50% of total counts of SWR events. Asterisks: red: 30%−group, green: 20%−group, blue 10%−group. Cells with asterisks are the same neurons marked in figure 4B.) (B) Average power of SWRs with (gray) or without (red) each neuron. (Asterisks: red: 30%−group, green: 20%−group, blue 10%−group.) (C) Distribution of power of all detected SWRs. (Top) Red SWRs with the activity of 30%−group. Gray: SWRs without the activity of 30%−group. (Middle) Green: SWRs with the activity of 20%−group. Gray SWRs without the activity of 20%−group. (Bottom) Blue: SWRs with the activity of 10%−group. Gray: SWRs without the activity of 20%−group.

Table 2.1. List of manufacturing materials

1-1. Tools

Item	Company	Model Number	Cost /quantity
Solidwork (CAD software)	Dassault Systemes, France		
3D printer	Formlabs, USA	Form 3	
Headstage	Neuralynx, USA	HS-18-LED	$1443.95/piece
Electrode interface board (EIB)		EIB-18	$104.7/piece
Thread-forming taps (M1.2 screws)	C.W.S.TOOLS, Belgium	DP2061105-M1.2 Threadformers M1.2	$54/piece

1-2. Consumables

Item	Company	Model Number	Cost /quantity	Quantity /device	Cost /device
Photopolymer resin	Formlabs, USA	RS-F2-GPBK-04 or RS-F2-GPGR-04	$149/L	1.20 cm^3	$1.8
Gold EIB pins	Neuralynx, USA	EIB Pins small	$0.16/piece	10 pieces	$1.6
Female-male breakaway header pins	Male pin: Digikey, USA	ED90328-ND	$0.16/piece	1 pair	$0.30
	Female socket: Farnell, UK	2840876	$0.14/piece		
PFA-coated stainless-steel wire	A-M system, USA	791400	$1.52/30.5cm	10cm	$0.50
Self-tapping bone screw	Fine Science Tools, Germany	19010-00	$0.88/piece	1 piece	$0.88
Polyimide tubing	Nordson, USA	141-0001	$0.20/30.5cm	10 cm	$0.07
23G tubing	Microgroup, USA	304 Hypo 23 Gauge Regular Wall (pre-cut length: 1.4cm)	$0.95/piece	3 pieces	$2.85
30G tubing		304 Hypo 30 Gauge Regular Wall (pre-cut length: 5.5cm)	$1.29/piece	3 pieces	$3.87
6mil stainless wire		304 Round Wire (pre-cut length: 8cm)	$0.98/piece	3 pieces	$2.94
Tetrode wire	Sandvik, Sweden	PX000004	$0.75/30.5cm	30 cm	$0.75
Polyimide-insulated stainless- steel wire	California Fine Wire, USA	.0005 STABLOHM 650	$0.85/30.5cm	10 cm	$0.30
UV-curable dental cement	SDI, Australia	Wave A2	$10.65/piece	1/2 piece	$5.33
M 1.2 screws	Micro-Modele, France	DIN84 M1.2x6	$0.30/piece	2 pieces	$0.60
Custom-made Microdrive screws (M1.2*0.25)	Advanced Machining & Tooling, Inc, USA	Design on file at AM&T, see [32]	$6.25/piece	3 pieces	$18.75
				Total cost	$40.54

	Recording duration (S)		No.of SWR		SWR Frequency (Hz)	
	Spontaneous	Disrupted	Spontaneous	Disrupted	Spontaneous	Disrupted
Animal 1	383.0	109.0	358.0	92.0	0.93	0.84
Animal 2	260.0	320.0	41.0	220.0	0.16	0.69
Animal 3	453.0	380.0	81.0	43.0	0.18	0.11
Animal 4	270.0	271.0	339.0	393.0	1.26	1.45

Table 2.2. Recording duration and SWR detection frequency from all animals

Chapter 3. Simultaneous cellular imaging and electrical recording for dissecting neuronal ensemble activity of SWR in multiple environments

Summary

In the previous chapter, we introduced our new device for simultaneous SWR recording by electrophysiological method and calcium imaging from hippocampal CA1 from freely behaving animals. Using this device, we could successfully demonstrated the effect of electrical SWR disruption recorded by neuronal calcium signals.

In this chapter, to investigate individual neuronal ensembles of SWRs, we demonstrated simultaneous dual recording approaches from behaving animals in two different contexts. By comparing active neurons during SWRs in two different spatial environment, we observed different frequency of SWRs by the environments and behavioral activity, and further identified that there are changes in the neuronal population consisting SWRs across environments. Our study suggests the potential of our microdrive array as a tool to investigate cellular composition of SWRs for memory encoding and consolidation.

Introduction

Sharp wave-ripples (SWRs) are characteristic brain activity pattern found in the hippocampus (Buzsaki, 1989, Buzsaki, 2015). This high-frequency (140-225Hz) pattern of the hippocampus encodes specific cellular spike ensembles (Taxidis et al., 2015), suggesting its role in memory consolidation by re-activating previously activated neurons called replay (Wilson & McNaughton, 1994; O'Neill et al., 2008; Gridchyn et al., 2020; Josselyn & Frankland, 2018). Decoding studies on the hippocampal replay activity showed that different subsets of hippocampal neurons consist sequential activity of replay depending on the type of memory and environment of the animal (Davidson et al., 2009; Michon et al., 2019; Gridchyn et al., 2020; Pfeiffer, 2020). However, as this replay phenomenon has been studied mainly using electrophysiological approaches, it was difficult to identify spatial location of individual neurons in the replay and trace them over time across conditions.

In our previous study, to observe SWRs with high spatial resolution as well as temporal resolution, we built a custom-designed microdrive array and demonstrated simultaneous observation of SWR from mice expressing the genetically encoded calcium sensor GCaMP6s.

In this study, using this recording system, we observed hippocampal CA1 signal of freely behaving animals in two different spatial context to investigate whether cellular activities consisting SWRs changes by the environments. From the result, we observed that different group of neuronal population showed increased activity after SWRs onset depending on the environment of the animals.

Our study not only shows changes in active neuronal population on the onset

of SWRs depending on the spatial contexts, but also suggests a potential use of our device in understanding neuronal composition of other fast and transient activity patterns in the brain.

Materials and Methods

Materials and methods in chapter 3 are identical to chapter 2, except behavioral environments and statistical analysis.

1. Behavioral environments

To compare neuronal activity of the animal in different environments, two spatially different contexts were prepared.

1) Open field: 20 cm long each side. Exploration time: approx. 3 minutes (Figure 3.1 A).

2) Linear track: 110 cm long (80cm of track with a 15cm x 15cm platform in each end). Exploration time: approx. 4 minutes (Figure 3.1 B).

Untrained and implanted animals were allowed to freely explore two different environments, with fixed time duration but without fixed order.

2. Statistics

To quantify the activity of cells during hippocampal SWRs, we computed the average $\Delta F/F$ cellular calcium responses to SWRs in a 1 second time window following SWR onset, relative to the average response in a 1 second window

pre-SWR onset. A bias score between two spatial contexts was calculated by computing the difference of the average SWR-related calcium responses (average ⊿F/F during 1 second window of post SWR - average ⊿F/F during 1 second window of pre SWR) in each context for every cell. A two-sample t-test was used to compare average SWR calcium response to the calcium response for randomly selected time points.

Results

Simultaneous electrophysiological recording and 1-photon imaging from freelymoving mice in two different contexts

In the first paradigm, animals (n=3, 1 session per animal) first explored a familiar arena (open field, 20 cm long sides) for 3 minutes (Figure 3.1 A), followed by running on a 110 cm long linear track for 4 minutes (Figure 3.1 B).

Animals were mostly quiet in the open field (Figure 3.1 C left, D left), associated with a high incidence of SWRs in the hippocampal LFP (Figure 3.1 E left, F left). On the linear track, animals were more active and ran a few laps (Figure 3.1 C right, D right). As expected, hippocampal LFP was characterized by theta oscillations as animals moved and SWRs as animals paused (Figure 3.1 E). The average ripple envelopes amplitude was higher in the open field than in the linear track. The average ripple rates was higher in the open field (average 0.60 Hz) than in the linear track (average 0.26 Hz) across all animals. Cellular calcium signals were acquired alongside the behavior and LFP (Figure 3.1 G).

Differential hippocampal calcium activity in two environments

Taking advantage of the simultaneous imaging of cell activity and LFP recording, we next looked at the change of calcium signals for each SWR event in each spatial context. SWR onsets and offsets were detected in the band-pass filtered (140-225 Hz) electrical signal, and SWRs with a duration between 60 ms-200 ms were selected for further analysis.

It has been reported that in the awake state, hippocampal place cells that encode the current environment are most strongly reactivated during SWRs (Carr et al., 2011; Olafsdottir et al., 2018). In addition, place cells show global remapping such that different environments are encoded by distinct place cell ensembles. Thus, we expect in our dataset that SWRs engage a largely separate set of cells in the open field and linear track. To test this prediction, cellular calcium responses during SWRs were calculated separately for the two spatial contexts (Figure 3.2 A, B). We found that largely separate subpopulations of cells were active during SWRs in the two spatial contexts. The average SWRs envelope had higher amplitude in the open field (Figure 3.2 C, black) as compared to the linear track (Figure 3.2 D, black). The SWR-triggered average calcium signal in the linear track (Figure 3.2 D, blue) lasted longer than in the open field (Figure 3.2 C, blue). Considering the multiunit activity on the linear track (Figure 3.2 D, red) was higher than in the open field (Figure 3.2 C, red), the long-lasting calcium signal on the linear track might not only include activity during SWRs but also other CA1 activity, i.e. place cells. The time course of the SWR-related average calcium signal outlasts the electrical SWR signature (Figure 3.2 C, D, blue), mainly because of the slower underlying calcium dynamics that are an indirect measurement of neuronal spiking and the properties of the calcium indicator (Chen et al.,

2013; Wei et al., 2020).

For all detected neurons (Figure 3.3A), we calculated the cellular calcium responses to SWRs in each spatial context separately (Figure 3.3 C). We computed a bias score defined as the difference of responses in the two contexts. While most cells were non-responsive during SWRs and had low bias score (i.e. close to 0) (Figure 3.3 C, grey), a subset of cells exhibited a higher SWR-related response in either the open field (Figure 3.3 C, red) or the linear track (Figure 3.3 C, blue). Cells were spatially intermingled regardless of their bias towards one or the other contexts (Figure 3.3 B).

Discussion

We demonstrated a successful recording of long-term electrophysiological data using tetrodes with 1-p calcium imaging in freely behaving animals in different behavioral environments. Our calcium transient data showed that in each environment, different subsets of hippocampal neurons show firing activity to SWRs detected in the LFP signals. The spatial identification of neurons suggest there are environment-specific hippocampal neurons showing different level of activation toward SWRs. Our simultaneous approach may improve decoding accuracy of hippocampal replay contents nested within SWRs to further investigate engram cells, the neurons encoding memory.

Replay of the hippocampal neurons are known to dwell in SWRs (Kudrimoti et al., 1999; Diba & Buzsaki, 2007). Neurons that were active during the acquisition process of information is found to show sequential activity again during resting state spontaneously, in a faster speed than in the acquisition period (Pfeiffer & Foster, 2013). As disruption of SWRs are critical in the

retention of memory, SWRs and replay is known to be involved in the memory consolidation process. However, due to its fast transient nature, it always has been investigated using electrophysiological methods for temporal information which had difficulties in identifying individual neurons across a long time. Using the device developed in Chapter 2, we could record SWRs with high temporal as well as spatial information, and successfully identified neurons that are active in two different conditions. Therefore, our results has a potential to improve identification of replay contents in both short-term and even can keep track of changes in the composition.

There is limitations in this study. Although animals are allowed to freely explore 2 different environments, but animals did not show same patterns of behavior; more silent and less mobile in the open field, and more locomotive on the linear track. Since SWRs are more frequent in the resting state, higher number of SWRs were detected in the open field environment than in the linear track. Therefore, active neurons within SWRs detected in the linear track environment does not show strong tendency as much as neurons from the open field. Also, in both environments, we recorded hippocampal activity in spontaneous state without any learning process. Therefore, SWRs recorded in both condition do not necessarily involved in the memory consolidation of specific tasks. However, since spontaneously occuring SWRs are known to be involved in the memory consolidation by replay of neurons, our approach is still valid to estimate and differentiate sequential activities of neurons within SWRs in different conditions, supported by spatial information, as well as conventional temporal information.

In summary, we implanted a new custom-designed microdrive array in the hippocampus and investigated calcium activity patterns in two different

environments from freely behaving animals. With further analysis, our data can potentially reveal individual cells and cellular ensembles that participate in SWRs, spatial/temporal connections of neurons, and their change over time to coordinate memories. Identifying cellular patterns would enable cell- or ensemble-specific SWRs disruption to uncover the detailed mechanism of memory formation.

Last but not least, although we introduced the application of our microdrive by recording hippocampal CA1 activity, it is not limited only to SWRs. With a modification of design and implant location, our microdrive array for dual approaches can also be broadly adopted to other brain regions to examine individual neuronal activities consisting of brain signals, such as slow oscillation in the cortex or theta oscillation in the medial septum. Also, multiple regional communication, such as sleep spindles-SWRs interaction in the cortico-hippocampal circuit, can be further investigated using our device.

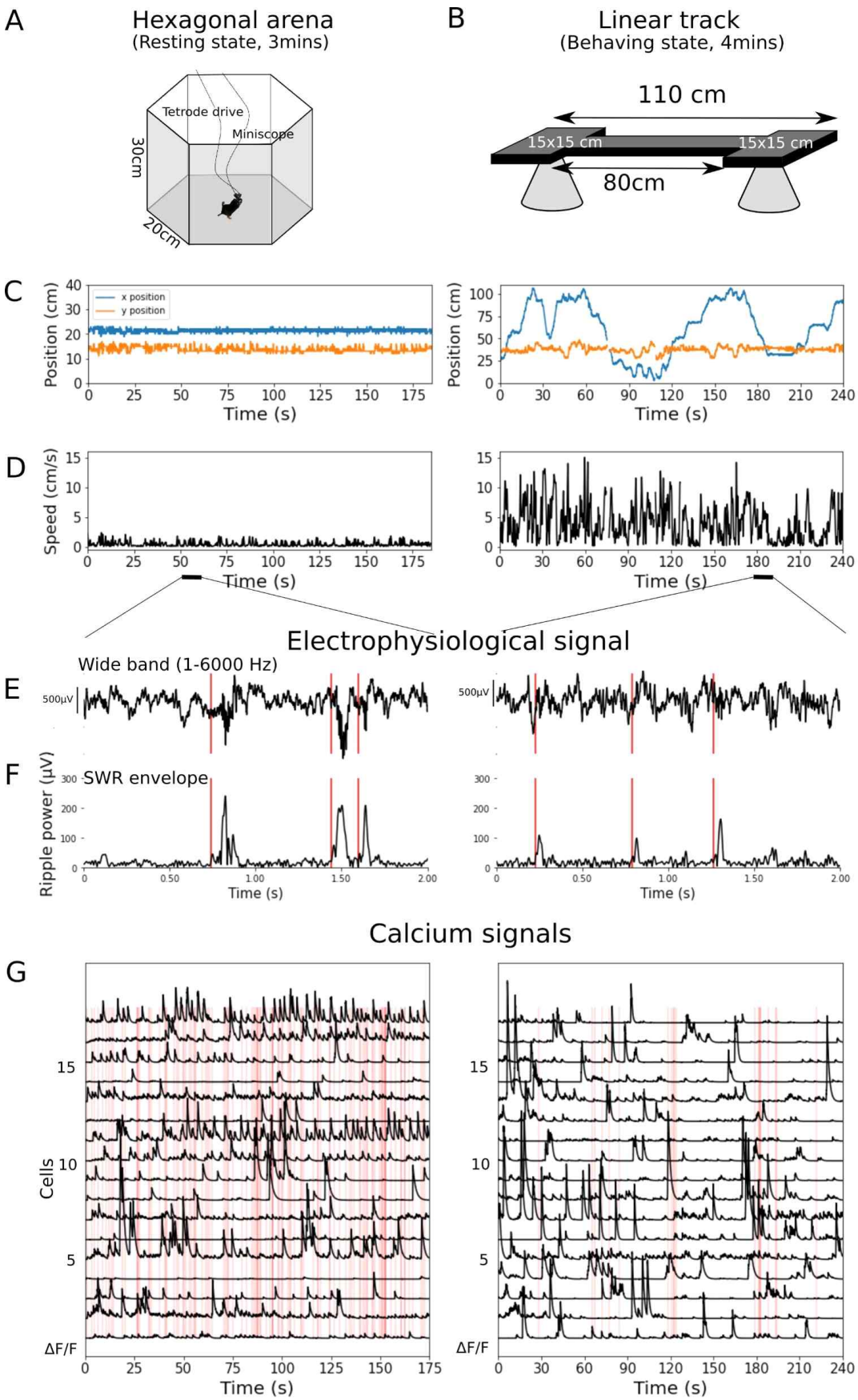
A
Hexagonal arena
(Resting state, 3mins)
Tetrode drive
Miniscope
30cm
20cm
B
Linear track
(Behaving state, 4mins)
110 cm
15x15 cm
15x15 cm
80cm
C
Position (cm)
x position
y position
Time (s)
D
Speed (cm/s)
Time (s)
Electrophysiological signal
E
Wide band (1-6000 Hz)
500µV
F
Ripple power (µV)
SWR envelope
Time (s)
Calcium signals
G
Cells
ΔF/F
Time (s)

Figure 3.1 Electrophysiological signals and calcium transient were simultaneously acquired in two spatial contexts from freely behaving animals. (A) Illustration of the open field. (B) Illustration of the linear track. (C) Position of animal in the open field (left) and on the linear track (right). Note that the animal is mainly quiet in the arena, and is more active on the linear track. (D) Speed of animal in the open field (left) and on the linear track (right). (E) Representative wide-band hippocampal LFP signal in the open field (left) and on the linear track (right). Vertical red lines indicate onset of offline detected SWRs. (F) Envelope of high frequency ripple activity of the signals in (E). (G) Calcium activity trace of relative fluorescence ($\Delta F/F$) from 17 example cells in the open field (left) and the linear track (right). Red lines: detected SWRs. Plotted cells are marked in Figure 5H.

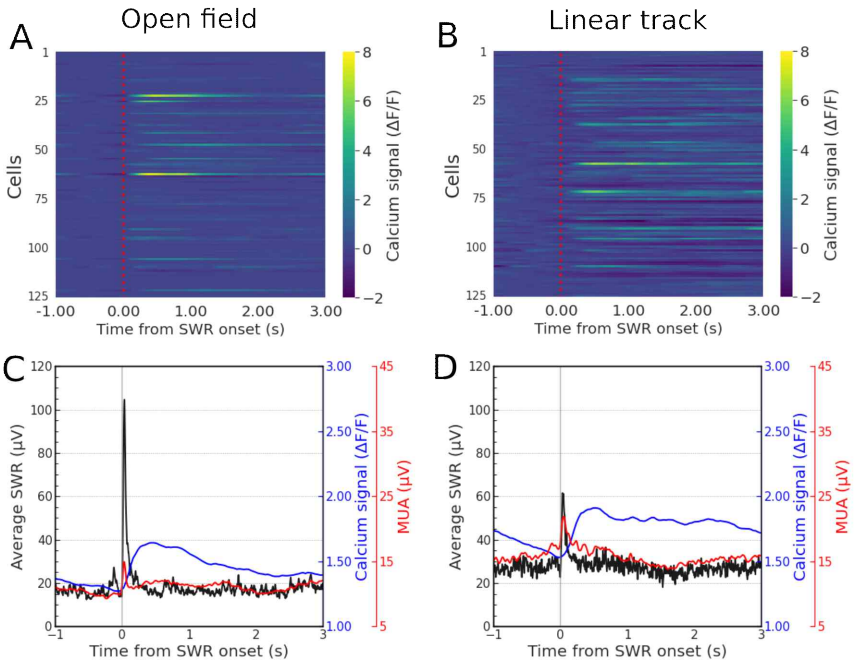

Figure 3.2. Neuronal calcium signals increase after onset of SWRs. Data from one mouse is shown. (A, B) SWR-triggered average calcium response from all cells in the open field (A), and on the linear track (B) (red: SWR onset). (C, D) SWR-triggered average of SWR power (black), calcium signal (blue), and absolute MUA power (red) in the open field (C), and on the linear track (D) (gray: SWR onset).

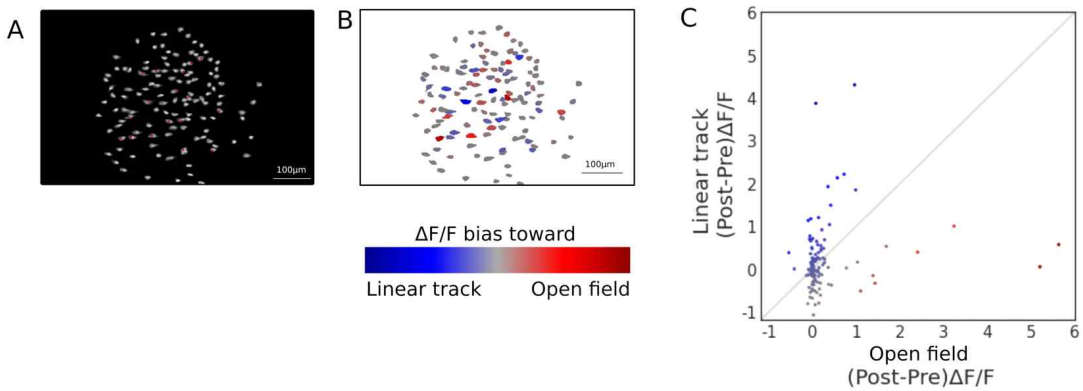

Figure 3.3. Different subsets of cells respond to SWRs depending on the behavioral state. (A) Frame of all detected cells superimposed by spatial information analysis. Red: neurons plotted in Figure 4.1 G (total of 125 cells window size: 450 μm* 700 μm). (B) Spatial location of cells colored with bias score, toward the open field (red) or linear track (blue). (total of 125 cells, window size: 450 μm* 700 μm). (C) Cellular calcium responses to SWRs on the open field or linear track. Colors denote the bias score of each cell, toward the open field (red) or linear track (blue).

Chapter 4. Conclusion and future perspective

In this study, we sought to understand how hippocampal neurons encode external information by investigating hippocampal sharp wave ripples in various methods from freely behaving animals. Hippocampal SWR is known to consist of a diverse subset of neurons depending on the given information, but due to its short duration, it has been investigated by electrophysiological method with high temporal resolution but without spatial information of neuronal location. To further understand the neuronal composition of SWRs with high temporal precision as well as a spatial relationship between neurons, in this research, we not only advanced in vivo SWRs acquisition techniques but also presented environment-specific activation of hippocampal neurons within SWRs demonstrated by 1-p calcium imaging data.

In the first part of the study (Chapter 2), we developed a new tetrode microdrive array for mice to collect the LFP signal of the hippocampus in combination with 1-photon calcium imaging, from freely behaving mice. To be able to use a mouse model for 1-p calcium imaging, it was critical to reduce the weight of the microdrive array so that animals can freely run the experimental setup without excessive pressure for long-term recording. It also has to carry out the acquisition of hippocampal LFP and disruption of SWRs via its connective fibers. To this end, using a 3D printer, we manufactured a new and durable microdrive array equipped with tetrodes and stimulus wire that can be combined with a 1-p calcium imaging device. Animals were implanted with our new microdrive array and UCLA miniscope, and hippocampal SWRs in vivo were recorded in spontaneous and disrupted conditions. Our results demonstrated that real-time electrophysiological disruption of SWRs was reflected in the calcium transient signals recorded

simultaneously. It was also observed that more neurons synchronously fire at SWR events compared to other time points, and neurons participate in SWRs at different occurrences rather than equally contribute, implying biased composition of neurons in SWRs. These results not only validate the temporal accuracy of the recording from the microdrive array with the 1-p calcium transients but also suggest that the composition of SWRs signals could be understood using our data.

In the second part of the study (Chapter 3), using this microdrive array with UCLA miniscope, we recorded hippocampal SWRs from freely behaving animals while animals are exploring different environments and compared their activities. Hippocampal LFP was recorded from both hippocampi using dual approaches simultaneously and the signals were compared by the acquisition environments of the animals. From the calcium transient data, we could identify a particular group of neurons firing more activity to SWRs onset. Furthermore, it was observed that certain subsets of neurons tend to fire more often in one environment than another, identified by the spatial location map of recorded neurons. Since hippocampal SWRs have a very short duration and are temporally transient, they have been recorded by the electrophysiological method, and the composition was presumed by decoding the signal. In this study, we recorded SWRs using calcium imaging and identified the spatial location of participating neurons individually, and showed the changes in the neuronal composition of the signal depending on the environments of the animal. Since hippocampal SWR is known to consolidate encoded hippocampal memory, there is a chance that neurons with biased activity shown in our study might be neurons encoding hippocampal memory, such as engram cells.

It is important to note that to compare SWRs between environmental conditions, we observed cellular firing activity on the onset of SWRs, not necessarily neuronal activity within SWRs time windows. Although calcium transient data is temporally synchronized to LFP data, calcium decay speed is not comparable to aligning with the fast transient signal of LFP. Therefore, we could not conclude that the neurons we observed in this study are firing within the SWRs window. For the next step of this project, I will focus on identifying individual cells and cellular ensembles that constitute SWRs, to understand how neurons are connected spatial and temporal, and how they change over time to coordinate memories.

For my next plan, to understand long-term memory formation between brain regions, I will apply our device to investigate the relationship between the neocortex and the hippocampus. In this study, we developed our microdrive array to investigate signals available only from the hippocampal CA1. However, as our design is highly flexible according to the regions of interest, it is not limited only to the hippocampus but can be broadly adopted to other regions to examine individual neuronal activities in multiple approaches, such as slow oscillation in the cortex or theta oscillation in the medial septum. Furthermore, multiple regional communication could be investigated using our dual approaches, such as sleep spindles-SWRs interaction in the cortico-hippocampal circuit.

The caveat of this study is that signals collected via electrophysiological approach and calcium imaging are recorded from two hippocampi from both hemispheres independently. A large body of literature shows the synchronous occurrence of SWR in both hippocampi, but there is a study that observed different timing of SWR in both hippocampi (Villette et al., 2017). Therefore,

there is a chance that SWR activities detected from the LFP data are not completely identical to the calcium signals. Second, due to technical limitations of the calcium imaging technique, the total recording time was relatively short, a maximum of 10 mins. Therefore, even though environment-specific activation of a subpopulation of cells is observed, our results may include not only environment-dependent activity but also internally-driven spontaneous activity changes over time (Han et al., 2007; Pastalkova et al., 2008).

Overall, we combined electrophysiological and calcium imaging methods to record hippocampal neuronal activities from freely behaving animals, and observed that hippocampal neurons have biased activities on the onset of hippocampal SWRs depending on the environmental context, demonstrating that hippocampal neurons encode and consolidate preferential information. Our study not only suggests improved identification of neurons in a fast and transient electrophysiological signal by augmenting spatial information of neurons but also may reveal temporal and spatial networks of neurons that constitute SWRs to understand how memory is inhabited in the hippocampus system.

References

Abadchi J, Nazari-Ahangarkolaee M, Gattas S, Bermudez-Contreras E, Luczak A, McNaughton B, Mohajerani M (2020). Spatiotemporal patterns of neocortical activity around hippocampal sharp-wave ripples. Elife, 9, e51972.

Abela, A. R., Duan, Y., & Chudasama, Y. (2015). Hippocampal interplay with the nucleus accumbens is critical for decisions about time. *European Journal of Neuroscience*, *42*(5), 2224-2233.

Aharoni, D., Khakh, B. S., Silva, A. J., & Golshani, P. (2019). All the light that we can see: a new era in miniaturized microscopy. *Nature methods*, *16*(1), 11-13.

Ahmed, O. J., & Mehta, M. R. (2009). The hippocampal rate code: anatomy, physiology and theory. *Trends in neurosciences*, *32*(6), 329-338. https://doi.org/10.1016/j.tins.2009.01.009

Allen, W. E., Chen, M. Z., Pichamoorthy, N., Tien, R. H., Pachitariu, M., Luo, L., & Deisseroth, K. (2019). Thirst regulates motivated behavior through modulation of brainwide neural population dynamics. *Science*, *364*(6437), eaav3932.

Alvarez P, Squire L (1994). Memory consolidation and the medial temporal lobe: a simple network model. Proceedings of the national academy of sciences, 91(15), 7041-7045.

Anderson, M. C., Bunce, J. G., & Barbas, H. (2016). Prefrontal-hippocampal pathways underlying inhibitory control over memory. *Neurobiology of learning and memory*, *134*, 145-161.

Atkinson, R. C., & Shiffrin, R. M. (1968). Human memory: A proposed system

and its control processes. In *Psychology of learning and motivation* (Vol. 2, pp. 89-195). Academic Press.

Bekkers, J. M. (2011). Pyramidal neurons. *Current biology*, *21*(24), R975.

Benito N, Martin-Vazquez G, Makarova J, Makarov V, Herreras O (2016). The right hippocampus leads the bilateral integration of gamma-parsed lateralized information. Elife, 5, e16658.

Berenyi, A., Somogyvari, Z., Nagy, A. J., Roux, L., Long, J. D., Fujisawa, S., ... & Buzsaki, G. (2014). Large-scale, high-density (up to 512 channels) recording of local circuits in behaving animals. *Journal of neurophysiology*, *111*(5), 1132-1149.

Burdakov, D., & Peleg-Raibstein, D. (2020). The hypothalamus as a primary coordinator of memory updating. *Physiology & Behavior*, *223*, 112988.

Bush, D., Barry, C., & Burgess, N. (2014). What do grid cells contribute to place cell firing?. *Trends in neurosciences*, *37*(3), 136-145.

Buzsaki, G. (1986). Hippocampal sharp waves: their origin and significance. *Brain research*, *398*(2), 242-252.

Buzsaki G (1989). Two-stage model of memory trace formation: a role for "noisy" brain states. Neuroscience, 31(3), 551-570.

Buzsaki, G. (2004). Large-scale recording of neuronal ensembles. *Nature neuroscience*, *7*(5), 446-451.

Buzsaki, G. (2015). Hippocampal sharp wave-ripple: A cognitive biomarker for episodic memory and planning. *Hippocampus*, *25*(10), 1073-1188.

Buzsaki G, Buhl D, Harris K, Csicsvari J, Czeh B, Morozov A (2003). Hippocampal network patterns of activity in the mouse. Neuroscience, 116(1),

201-211.

Buzsaki, G., & Chrobak, J. J. (2005). Synaptic plasticity and self-organization in the hippocampus. *Nature neuroscience*, *8*(11), 1418-1420.

Buzsaki, G., Horvath, Z., Urioste, R., Hetke, J., & Wise, K. (1992). High-frequency network oscillation in the hippocampus. *Science*, *256*(5059), 1025-1027.

Buzsaki, G., Stark, E., Berenyi, A., Khodagholy, D., Kipke, D. R., Yoon, E., & Wise, K. D. (2015). Tools for probing local circuits: high-density silicon probes combined with optogenetics. *Neuron*, *86*(1), 92-105.

Cai, D. J., Aharoni, D., Shuman, T., Shobe, J., Biane, J., Song, W., ... & Silva, A. J. (2016). A shared neural ensemble links distinct contextual memories encoded close in time. *Nature*, *534*(7605), 115-118.

Camina, E., & Guell, F. (2017). The neuroanatomical, neurophysiological and psychological basis of memory: Current models and their origins. *Frontiers in pharmacology*, *8*, 438.

Carr, M. F., Jadhav, S. P., & Frank, L. M. (2011). Hippocampal replay in the awake state: a potential substrate for memory consolidation and retrieval. *Nature neuroscience*, *14*(2), 147-153.

Chen, R., Canales, A., & Anikeeva, P. (2017). Neural recording and modulation technologies. *Nature Reviews Materials*, *2*(2), 1-16.

Chen, S., He, L., Huang, A. J., Boehringer, R., Robert, V., Wintzer, M. E., ... & McHugh, T. J. (2020). A hypothalamic novelty signal modulates hippocampal memory. *Nature*, *586*(7828), 270-274.

Chen T, Wardill T, Sun Y, Pulver S, Renninger S, Baohan A, Schreiter E, Kerr

R, Orger M, Jayaraman V, Looger L, Svoboda K, Kim D (2013). Ultrasensitive fluorescent proteins for imaging neuronal activity. Nature, 499(7458), 295-300.

Chenkov, N. A. (2017). Network Mechanisms Underlying Sharp-Wave Ripples and Memory Replay: GABAergic Modulation of Sharp-Wave Ripples Incidence (Doctoral dissertation, Humboldt Universitaet zu Berlin (Germany)).

Chrobak, J. J., & Buzsaki, G. (1996). High-frequency oscillations in the output networks of the hippocampal-entorhinal axis of the freely behaving rat. Journal of neuroscience, 16(9), 3056-3066.

Ciliberti, D., & Kloosterman, F. (2017). Falcon: a highly flexible open-source software for closed-loop neuroscience. *Journal of neural engineering*, *14*(4), 045004.

Colgin, L. L. (2016). Rhythms of the hippocampal network. *Nature Reviews Neuroscience*, *17*(4), 239-249.

Cox, R., Ruber, T., Staresina, B. P., & Fell, J. (2020). Sharp wave-ripples in human amygdala and their coordination with hippocampus during NREM sleep. Cerebral cortex communications, 1(1), tgaa051.

Csicsvari, J., Hirase, H., Czurko, A., Mamiya, A., & Buzsaki, G. (1999). Oscillatory coupling of hippocampal pyramidal cells and interneurons in the behaving rat. Journal of Neuroscience, 19(1), 274-287.

Csicsvari, J., Jamieson, B., Wise, K. D., & Buzsaki, G. (2003). Mechanisms of gamma oscillations in the hippocampus of the behaving rat. *Neuron*, *37*(2), 311-322.

Czurko, A., Hirase, H., Csicsvari, J., & Buzsaki, G. (1999). Sustained

activation of hippocampal pyramidal cells by ‘space clamping’ in a running wheel. *European Journal of Neuroscience*, *11*(1), 344-352.

Davidson, T. J., Kloosterman, F., & Wilson, M. A. (2009). Hippocampal replay of extended experience. *Neuron*, *63*(4), 497-507.

Dana H, Chen T, Hu A, Shields B, Guo C, Looger L, Kim D, Svoboda K (2014). Thy1-GCaMP6 transgenic mice for neuronal population imaging in vivo. PloS one, 9(9), e108697

de Groot, A., van den Boom, B. J., van Genderen, R. M., Coppens, J., van Veldhuijzen, J., Bos, J., ... & Hoogland, T. M. (2020). NINscope, a versatile miniscope for multi-region circuit investigations. *Elife*, *9*, e49987.

Diba, K., & Buzsaki, G. (2007). Forward and reverse hippocampal place-cell sequences during ripples. *Nature neuroscience*, *10*(10), 1241-1242.

Diekelmann, S., & Born, J. (2010). The memory function of sleep. *Nature Reviews Neuroscience*, *11*(2), 114-126.

Diekelmann, S., Born, J., & Wagner, U. (2010). Sleep enhances false memories depending on general memory performance. *Behavioural brain research*, *208*(2), 425-429.

Dordek, Y., Soudry, D., Meir, R., & Derdikman, D. (2016). Extracting grid cell characteristics from place cell inputs using non-negative principal component analysis. *Elife*, *5*, e10094.

Duncan, K., Doll, B. B., Daw, N. D., & Shohamy, D. (2018). More than the sum of its parts: a role for the hippocampus in configural reinforcement learning. *Neuron*, *98*(3), 645-657.

Dupret D, O'neill J, Pleydell-Bouverie B, Csicsvari J (2010). The

reorganization and reactivation of hippocampal maps predict spatial memory performance. Nature neuroscience, 13(8), 995.

Ego-Stengel, V., & Wilson, M. A. (2010). Disruption of ripple-associated hippocampal activity during rest impairs spatial learning in the rat. *Hippocampus*, *20*(1), 1-10.

Eichenbaum, H. (2017). Prefrontal-hippocampal interactions in episodic memory. *Nature Reviews Neuroscience*, *18*(9), 547-558.

Eichenbaum, H., & Cohen, N. J. (2004). *From conditioning to conscious recollection: Memory systems of the brain* (No. 35). Oxford University Press on Demand.

Ellenbogen, J. M., Hu, P. T., Payne, J. D., Titone, D., & Walker, M. P. (2007). Human relational memory requires time and sleep. *Proceedings of the National Academy of Sciences*, *104*(18), 7723-7728.

Emiliani, V., Cohen, A. E., Deisseroth, K., & H□usser, M. (2015). All-optical interrogation of neural circuits. *Journal of Neuroscience*, *35*(41), 13917-13926.

Evangelista, R., Cano, G., Cooper, C., Schmitz, D., Maier, N., & Kempter, R. (2020). Generation of sharp wave-ripple events by disinhibition. Journal of Neuroscience, 40(41), 7811-7836.

Fernandez-Ruiz, A., Oliva, A., Fermino de Oliveira, E., Rocha-Almeida, F., Tingley, D., & Buzsaki, G. (2019). Long-duration hippocampal sharp wave ripples improve memory. *Science*, *364*(6445), 1082-1086.

Fernandez-Ruiz A, Oliva A, Nagy G, Maurer A, Berenyi A, Buzsaki G (2017). Entorhinal-CA3 dual-input control of spike timing in the hippocampus by

theta-gamma coupling. Neuron, 93(5), 1213-1226.

Foster T, Castro C, McNaughton B (1989). Spatial selectivity of rat hippocampal neurons: dependence on preparedness for movement. Science, 244(4912), 1580-1582.

Foster, D. J., & Wilson, M. A. (2006). Reverse replay of behavioural sequences in hippocampal place cells during the awake state. *Nature*, *440*(7084), 680-683.

Frankland, P. W., Kohler, S., & Josselyn, S. A. (2013). Hippocampal neurogenesis and forgetting. *Trends in neurosciences*, *36*(9), 497-503.

Frankland, P. W., Josselyn, S. A., & Kohler, S. (2019). The neurobiological foundation of memory retrieval. *Nature neuroscience*, *22*(10), 1576-1585.

Furtak, S. C., Wei, S. M., Agster, K. L., & Burwell, R. D. (2007). Functional neuroanatomy of the parahippocampal region in the rat: the perirhinal and postrhinal cortices. *Hippocampus*, *17*(9), 709-722.

Fyhn, M., Hafting, T., Treves, A., Moser, M. B., & Moser, E. I. (2007). Hippocampal remapping and grid realignment in entorhinal cortex. *Nature*, *446*(7132), 190-194.

Girardeau G, Benchenane K, Wiener S, Buzsaki G, Zugaro M (2009). Selective suppression of hippocampal ripples impairs spatial memory. Nature neuroscience, 12(10), 1222-1223.

Girardeau, G., & Zugaro, M. (2011). Hippocampal ripples and memory consolidation. *Current opinion in neurobiology*, *21*(3), 452-459.

Graves, A. R., Moore, S. J., Bloss, E. B., Mensh, B. D., Kath, W. L., & Spruston, N. (2012). Hippocampal pyramidal neurons comprise two distinct cell types

that are countermodulated by metabotropic receptors. *Neuron*, *76*(4), 776-789.

Gray, C. M., Maldonado, P. E., Wilson, M., & McNaughton, B. (1995). Tetrodes markedly improve the reliability and yield of multiple single-unit isolation from multi-unit recordings in cat striate cortex. *Journal of neuroscience methods*, *63*(1-2), 43-54.

Gridchyn I, Schoenenberger P, O' Neill J, Csicsvari J (2020). Assembly-specific disruption of hippocampal replay leads to selective memory deficit. Neuron.

Gupta, A. S., Van Der Meer, M. A., Touretzky, D. S., & Redish, A. D. (2010). Hippocampal replay is not a simple function of experience. *Neuron*, *65*(5), 695-705.

Hafting, T., Fyhn, M., Molden, S., Moser, M. B., & Moser, E. I. (2005). Microstructure of a spatial map in the entorhinal cortex. *Nature*, *436*(7052), 801-806.

HajjHassan, M., Chodavarapu, V., & Musallam, S. (2008). NeuroMEMS: neural probe microtechnologies. *Sensors*, *8*(10), 6704-6726.

Harris, K. D., Csicsvari, J., Hirase, H., Dragoi, G., & Buzsaki, G. (2003). Organization of cell assemblies in the hippocampus. *Nature*, *424*(6948), 552-556.

Haufler, D., & Pare, D. (2014). High-frequency oscillations are prominent in the extended amygdala. Journal of neurophysiology, 112(1), 110-119.

Hirase, H., Czurko, A., Csicsvari, J., & Buzsaki, G. (1999). Firing rate and theta-phase coding by hippocampal pyramidal neurons during 'space

clamping’. *European Journal of Neuroscience*, *11*(12), 4373-4380.

Hirase, H., Leinekugel, X., Czurko, A., Csicsvari, J., & Buzsaki, G. (2001). Firing rates of hippocampal neurons are preserved during subsequent sleep episodes and modified by novel awake experience. *Proceedings of the National Academy of Sciences*, *98*(16), 9386-9390.

Hong, G., & Lieber, C. M. (2019). Novel electrode technologies for neural recordings. *Nature Reviews Neuroscience*, *20*(6), 330-345.

Hunt D, Linaro D, Si B, Romani S, Spruston N (2018). A novel pyramidal cell type promotes sharp-wave synchronization in the hippocampus. Nature neuroscience, 21(7), 985-995.

Han, J. H., Kushner, S. A., Yiu, A. P., Cole, C. J., Matynia, A., Brown, R. A., ... & Josselyn, S. A. (2007). Neuronal competition and selection during memory formation. science, 316(5823), 457-460.

Ito, R., Robbins, T. W., Pennartz, C. M., & Everitt, B. J. (2008). Functional interaction between the hippocampus and nucleus accumbens shell is necessary for the acquisition of appetitive spatial context conditioning. *Journal of Neuroscience*, *28*(27), 6950-6959.

Jacobs, J. (2014). Hippocampal theta oscillations are slower in humans than in rodents: implications for models of spatial navigation and memory. *Philosophical Transactions of the Royal Society B: Biological Sciences*, *369*(1635), 20130304.

Jadhav S, Kemere C, German P, Frank L (2012). Awake hippocampal sharp-wave ripples support spatial memory. Science, 336(6087), 1454-1458.

Jarosiewicz, B., McNaughton, B. L., & Skaggs, W. E. (2002). Hippocampal

population activity during the small-amplitude irregular activity state in the rat. *Journal of Neuroscience*, *22*(4), 1373-1384.

Ji, D., & Wilson, M. A. (2007). Coordinated memory replay in the visual cortex and hippocampus during sleep. *Nature neuroscience*, *10*(1), 100-107.

Joo, H. R., & Frank, L. M. (2018). The hippocampal sharp wave-ripple in memory retrieval for immediate use and consolidation. *Nature Reviews Neuroscience*, *19*(12), 744-757.

Josselyn S, Frankland P (2018). Memory allocation: mechanisms and function. Annual review of neuroscience, 41, 389-413.

Josselyn, S. A., Kohler, S., & Frankland, P. W. (2015). Finding the engram. *Nature Reviews Neuroscience*, *16*(9), 521-534.

Josselyn, S. A., & Tonegawa, S. (2020). Memory engrams: Recalling the past and imagining the future. *Science*, *367*(6473), eaaw4325.

Kandel E (2007). In search of memory: The emergence of a new science of mind. WW Norton & Company.

Kandel, E. R., Dudai, Y., & Mayford, M. R. (2014). The molecular and systems biology of memory. *Cell*, *157*(1), 163-186.

Khakpai, F., Nasehi, M., Haeri-Rohani, A., Eidi, A., & Zarrindast, M. R. (2013). Septo-hippocampo-septal loop and memory formation. *Basic and clinical neuroscience*.

Klausberger, T., Magill, P. J., Marton, L. F., Roberts, J. D. B., Cobden, P. M., Buzsaki, G., & Somogyi, P. (2003). Brain-state-and cell-type-specific firing of hippocampal interneurons in vivo. Nature, 421(6925), 844-848.

Klinzing, J. G., Niethard, N., & Born, J. (2019). Mechanisms of systems

memory consolidation during sleep. *Nature neuroscience*, *22*(10), 1598–1610.

Kloosterman F, Davidson T, Gomperts S, Layton S, Hale G, Nguyen D, Wilson M (2009). Micro-drive array for chronic in vivo recording: drive fabrication. JoVE (Journal of Visualized Experiments), (26), e1094.

Kohus, Z., Kali, S., Rovira-Esteban, L., Schlingloff, D., Papp, O., Freund, T. F., ... & Gulyas, A. I. (2016). Properties and dynamics of inhibitory synaptic communication within the CA3 microcircuits of pyramidal cells and interneurons expressing parvalbumin or cholecystokinin. The Journal of physiology, 594(13), 3745-3774.

Kragel, J. E., VanHaerents, S., Templer, J. W., Schuele, S., Rosenow, J. M., Nilakantan, A. S., & Bridge, D. J. (2020). Hippocampal theta coordinates memory processing during visual exploration. *Elife*, *9*.

Kraushaar, U., & Jonas, P. (2000). Efficacy and stability of quantal GABA release at a hippocampal interneuron-principal neuron synapse. Journal of Neuroscience, 20(15), 5594-5607.

Kudrimoti, H. S., Barnes, C. A., & McNaughton, B. L. (1999). Reactivation of hippocampal cell assemblies: effects of behavioral state, experience, and EEG dynamics. *Journal of Neuroscience*, *19*(10), 4090-4101.

LeGates, T. A., Kvarta, M. D., Tooley, J. R., Francis, T. C., Lobo, M. K., Creed, M. C., & Thompson, S. M. (2018). Reward behaviour is regulated by the strength of hippocampus–nucleus accumbens synapses. *Nature*, *564*(7735), 258-262.

Lewis, P. A., & Durrant, S. J. (2011). Overlapping memory replay during sleep builds cognitive schemata. *Trends in cognitive sciences*, *15*(8), 343-351.

Lisman, J. E., & Grace, A. A. (2005). The hippocampal–VTA loop: controlling the entry of information into long–term memory. *Neuron*, *46*(5), 703–713.

Liu, X., Ramirez, S., Pang, P. T., Puryear, C. B., Govindarajan, A., Deisseroth, K., & Tonegawa, S. (2012). Optogenetic stimulation of a hippocampal engram activates fear memory recall. *Nature*, *484*(7394), 381–385.

Maren, S. (2008). Pavlovian fear conditioning as a behavioral assay for hippocampus and amygdala function: cautions and caveats. *European Journal of Neuroscience*, *28*(8), 1661–1666.

Marshall, L., & Born, J. (2007). The contribution of sleep to hippocampus–dependent memory consolidation. *Trends in cognitive sciences*, *11*(10), 442–450.

Marshel, J. H., Kim, Y. S., Machado, T. A., Quirin, S., Benson, B., Kadmon, J., ... & Deisseroth, K. (2019). Cortical layer–specific critical dynamics triggering perception. *Science*, *365*(6453), eaaw5202.

Matsumoto, N., Kitanishi, T., & Mizuseki, K. (2019). The subiculum: Unique hippocampal hub and more. *Neuroscience Research*, *143*, 1–12.

McClelland J, McNaughton B, O'Reilly R (1995). Why there are complementary learning systems in the hippocampus and neocortex: insights from the successes and failures of connectionist models of learning and memory. Psychological review, 102(3), 419.

McGaugh, J. L. (1966). Time–Dependent Processes in Memory Storage: Recent studies of learning and memory indicate that memory storage involves time–dependent processes. *Science*, *153*(3742), 1351–1358.

McGaugh, J. L. (2000). Memory––a century of consolidation. *Science*,

287(5451), 248-251.

McNamara, C. G., Tejero-Cantero, A., Trouche, S., Campo-Urriza, N., & Dupret, D. (2014). Dopaminergic neurons promote hippocampal reactivation and spatial memory persistence. *Nature neuroscience*, *17*(12), 1658-1660.

Michon F, Sun J, Kim C, Ciliberti D, Kloosterman F (2019). Post-learning hippocampal replay selectively reinforces spatial memory for highly rewarded locations. Current Biology, 29(9), 1436-1444.

Milner B, Squire L, Kandel E (1998). Cognitive neuroscience and the study of memory. Neuron, 20(3), 445-468.

Moretti, P., Levenson, J. M., Battaglia, F., Atkinson, R., Teague, R., Antalffy, B., ... & Zoghbi, H. Y. (2006). Learning and memory and synaptic plasticity are impaired in a mouse model of Rett syndrome. *Journal of Neuroscience*, *26*(1), 319-327.

Moscovitch, M., Cabeza, R., Winocur, G., & Nadel, L. (2016). Episodic memory and beyond: the hippocampus and neocortex in transformation. *Annual review of psychology*, *67*, 105.

Ngo, H. V., Fell, J., & Staresina, B. (2020). Sleep spindles mediate hippocampal-neocortical coupling during long-duration ripples. *elife*, *9*.

Nguyen D, Layton S, Hale G, Gomperts S, Davidson T, Kloosterman F, Wilson M (2009). Micro-drive Array for Chronic in vivo Recording: Tetrode Assembly. J. Vis. Exp. (26), e1098.

Norman, Y., Yeagle, E. M., Khuvis, S., Harel, M., Mehta, A. D., & Malach, R. (2019). Hippocampal sharp-wave ripples linked to visual episodic recollection in humans. *Science*, *365*(6454), eaax1030.

Nunez, A., & Buno, W. (2021). The theta rhythm of the hippocampus: From neuronal and circuit mechanisms to behavior. *Frontiers in Cellular Neuroscience*, *15*, 649262.

Okamoto, K., Ishikawa, T., Abe, R., Ishikawa, D., Kobayashi, C., Mizunuma, M., ... & Ikegaya, Y. (2014). Ex vivo cultured neuronal networks emit in vivo-like spontaneous activity. *The Journal of Physiological Sciences*, *64*(6), 421-431.

O'keefe, J., & Nadel, L. (1978). The hippocampus as a cognitive map.

O'Keefe, J., & Dostrovsky, J. (1971). The hippocampus as a spatial map: Preliminary evidence from unit activity in the freely-moving rat. *Brain research*.

Olafsdottir, H. F., Bush, D., & Barry, C. (2018). The role of hippocampal replay in memory and planning. *Current Biology*, *28*(1), R37-R50.

O'Mara, S. (2005). The subiculum: what it does, what it might do, and what neuroanatomy has yet to tell us. *Journal of anatomy*, *207*(3), 271-282.

O'Neill J, Senior T, Allen K, Huxter J, Csicsvari J (2008). Reactivation of experience-dependent cell assembly patterns in the hippocampus. Nature neuroscience, 11(2), 209-215.

Packard, M. G., & McGaugh, J. L. (1996). Inactivation of hippocampus or caudate nucleus with lidocaine differentially affects expression of place and response learning. *Neurobiology of learning and memory*, *65*(1), 65-72.

Peigneux, P., Laureys, S., Fuchs, S., Collette, F., Perrin, F., Reggers, J., ... & Maquet, P. (2004). Are spatial memories strengthened in the human hippocampus during slow wave sleep?. *Neuron*, *44*(3), 535-545.

Pesaran, B., Vinck, M., Einevoll, G. T., Sirota, A., Fries, P., Siegel, M., ... &

Srinivasan, R. (2018). Investigating large-scale brain dynamics using field potential recordings: analysis and interpretation. *Nature neuroscience*, *21*(7), 903-919.

Pfeiffer, B. E. (2020). The content of hippocampal "replay". Hippocampus, 30(1), 6-18.

Pfeiffer, B. E., & Foster, D. J. (2013). Hippocampal place-cell sequences depict future paths to remembered goals. *Nature*, *497*(7447), 74-79.

Ponomarenko, A. A., Korotkova, T. M., & Haas, H. L. (2003). High frequency (200 Hz) oscillations and firing patterns in the basolateral amygdala and dorsal endopiriform nucleus of the behaving rat. Behavioural brain research, 141(2), 123-129.

Poo, M. M., Pignatelli, M., Ryan, T. J., Tonegawa, S., Bonhoeffer, T., Martin, K. C., ... & Stevens, C. (2016). What is memory? The present state of the engram. *BMC biology*, *14*(1), 1-18.

Pnevmatikakis E, Soudry D, Gao Y, Machado T, Merel J, Pfau D, Reardon T, Mu Y, Lacefield C, Yang W, Ahrens M, Bruno R, Jessell T, Peterka D, Yuste R, Paninski L (2016). Simultaneous denoising, deconvolution, and demixing of calcium imaging data. Neuron, 89(2), 285-299.

Preston, A. R., & Eichenbaum, H. (2013). Interplay of hippocampus and prefrontal cortex in memory. *Current biology*, *23*(17), R764-R773.

Preston, A. R., & Wagner, A. D. (2007). The medial temporal lobe and memory. In *Neurobiology of learning and memory* (pp. 305-337). Academic Press.

Ramadan W, Eschenko O, Sara S (2009). Hippocampal sharp wave/ripples

during sleep for consolidation of associative memory. PloS one, 4(8), e6697.

Rasch, B., & Born, J. (2008). Reactivation and consolidation of memory during sleep. *Current Directions in Psychological Science*, *17*(3), 188-192.

Rasch, B., & Born, J. (2013). About sleep's role in memory. *Physiological reviews*.

Resendez, S. L., Jennings, J. H., Ung, R. L., Namboodiri, V. M. K., Zhou, Z. C., Otis, J. M., ... & Stuber, G. D. (2016). Visualization of cortical, subcortical and deep brain neural circuit dynamics during naturalistic mammalian behavior with head-mounted microscopes and chronically implanted lenses. *Nature protocols*, *11*(3), 566-597.

Roesler, R., & McGaugh, J. L. (2019). Memory consolidation.

Roux L, Hu B, Eichler R, Stark E, Buzsaki G (2017). Sharp wave ripples during learning stabilize the hippocampal spatial map. Nature neuroscience, 20(6), 845-853.

Russell, L. E., Dalgleish, H. W., Nutbrown, R., Gauld, O. M., Herrmann, D., Fişek, M., ... & H□usser, M. (2022). All-optical interrogation of neural circuits in behaving mice. *Nature Protocols*, 1-42.

Ryan, T. J., Roy, D. S., Pignatelli, M., Arons, A., & Tonegawa, S. (2015). Engram cells retain memory under retrograde amnesia. *Science*, *348*(6238), 1007-1013.

Schonauer, M., Alizadeh, S., Jamalabadi, H., Abraham, A., Pawlizki, A., & Gais, S. (2017). Decoding material-specific memory reprocessing during sleep in humans. *Nature communications*, *8*(1), 1-9.

Schreiner, T., Petzka, M., Staudigl, T., & Staresina, B. P. (2021). Endogenous

memory reactivation during sleep in humans is clocked by slow oscillation–spindle complexes. *Nature communications*, *12*(1), 1–10.

Scott B, Thiberge S, Guo C, Tervo D, Brody C, Karpova A, Tank D (2018). Imaging cortical dynamics in GCaMP transgenic rats with a head–mounted widefield macroscope. Neuron, 100(5), 1045–1058.

Scoville, W. B., & Milner, B. (1957). Loss of recent memory after bilateral hippocampal lesions. *Journal of neurology, neurosurgery, and psychiatry*, *20*(1), 11.

Shin, J. D., Tang, W., & Jadhav, S. P. (2019). Dynamics of awake hippocampal–prefrontal replay for spatial learning and memory–guided decision making. *Neuron*, *104*(6), 1110–1125.

Shinohara Y, Hosoya A, Hirase H (2013). Experience enhances gamma oscillations and interhemispheric asymmetry in the hippocampus. Nature communications, 4(1), 1–10.

Sigurdsson, T., & Duvarci, S. (2016). Hippocampal–prefrontal interactions in cognition, behavior and psychiatric disease. *Frontiers in systems neuroscience*, *9*, 190.

Sinefeld, D., Xia, F., Wang, M., Wang, T., Wu, C., Yang, X., ... & Xu, C. (2022). Three–Photon Adaptive Optics for Mouse Brain Imaging. *Frontiers in neuroscience*, 774.

Skaggs, W. E., & McNaughton, B. L. (1996). Replay of neuronal firing sequences in rat hippocampus during sleep following spatial experience. *Science*, *271*(5257), 1870–1873.

Spruston, N. (2008). Pyramidal neurons: dendritic structure and synaptic

integration. *Nature Reviews Neuroscience*, *9*(3), 206-221.

Staba, R. J., Wilson, C. L., Bragin, A., Fried, I., & Engel Jr, J. (2002). Quantitative analysis of high-frequency oscillations (80-500 Hz) recorded in human epileptic hippocampus and entorhinal cortex. Journal of neurophysiology, 88(4), 1743-1752.

Staff, N. P., Jung, H. Y., Thiagarajan, T., Yao, M., & Spruston, N. (2000). Resting and active properties of pyramidal neurons in subiculum and CA1 of rat hippocampus. *Journal of neurophysiology*, *84*(5), 2398-2408.

Stamatakis A, Schachter M, Gulati S., Zitelli K, Malanowski S, Tajik A, Fritz C, Trulson M, Otte, S (2018). Simultaneous optogenetics and cellular resolution calcium imaging during active behavior using a miniaturized microscope. Frontiers in neuroscience, 12, 496.

Staresina, B. P., Bergmann, T. O., Bonnefond, M., Van Der Meij, R., Jensen, O., Deuker, L., ... & Fell, J. (2015). Hierarchical nesting of slow oscillations, spindles and ripples in the human hippocampus during sleep. Nature neuroscience, 18(11), 1679-1686.

Strange, B. A., Witter, M. P., Lein, E. S., & Moser, E. I. (2014). Functional organization of the hippocampal longitudinal & Milner, B. (1957). Loss of recent memory after bilateral hippocampal axis. *Nature Reviews Neuroscience*, *15*(10), 655-669.

Squire, L. R., Stark, C. E., & Clark, R. E. (2004). The medial temporal lobe. *Annu. Rev. Neurosci.*, *27*, 279-306.

Squire, L. R., & Zola, S. M. (1996). Structure and function of declarative and nondeclarative memory systems. *Proceedings of the National Academy of Sciences*, *93*(24), 13515-13522.

Suzuki S, Smith G (1987). Spontaneous EEG spikes in the normal hippocampus. I. Behavioral correlates, laminar profiles and bilateral synchrony. Electroencephalography and clinical neurophysiology, 67(4), 348-359.

Tang W, Jadhav S (2019). Sharp-wave ripples as a signature of hippocampal-prefrontal reactivation for memory during sleep and waking states. Neurobiology of learning and memory, 160, 11-20.

Takashima, A., Petersson, K. M., Rutters, F., Tendolkar, I., Jensen, O., Zwarts, M. J., ... & Fernandez, G. (2006). Declarative memory consolidation in humans: a prospective functional magnetic resonance imaging study. *Proceedings of the National Academy of Sciences*, *103*(3), 756-761.

Takeuchi, S., Suzuki, T., Mabuchi, K., & Fujita, H. (2003). 3D flexible multichannel neural probe array. *Journal of micromechanics and microengineering*, *14*(1), 104.

Takeuchi, T., Duszkiewicz, A. J., Sonneborn, A., Spooner, P. A., Yamasaki, M., Watanabe, M., ... & Morris, R. G. (2016). Locus coeruleus and dopaminergic consolidation of everyday memory. *Nature*, *537*(7620), 357-362.

Taxidis J, Anastassiou C, Diba K, Koch C (2015). Local field potentials encode place cell ensemble activation during hippocampal sharp wave ripples. Neuron, 87(3), 590-604.

Tonegawa, S., Pignatelli, M., Roy, D. S., & Ryan, T. J. (2015). Memory engram storage and retrieval. *Current opinion in neurobiology*, *35*, 101-109.

Tottenham, N., & Sheridan, M. A. (2010). A review of adversity, the amygdala and the hippocampus: a consideration of developmental timing. *Frontiers in human neuroscience*, 68.

Trevathan J, Asp A, Nicolai E, Trevathan J, Kremer N, Kozai T, Cheng D, Schachter M, Nassi J, Otte S, Parker J, Lujan J, Ludwig K. (2020). Calcium imaging in freely-moving mice during electrical stimulation of deep brain structures. bioRxiv, 460220.

Vago, D. R., & Kesner, R. P. (2008). Disruption of the direct perforant path input to the CA1 subregion of the dorsal hippocampus interferes with spatial working memory and novelty detection. *Behavioural brain research*, *189*(2), 273-283.

Valeeva G, Nasretdinov A, Rychkova V, Khazipov R (2019). Bilateral Synchronization of Hippocampal Early Sharp Waves in Neonatal Rats. Frontiers in Cellular Neuroscience, 13, 29.

Vanderwolf, C. H. (1969). Hippocampal electrical activity and voluntary movement in the rat. *Electroencephalography and clinical neurophysiology*, *26*(4), 407-418.

Van Strien, N. M., Cappaert, N. L. M., & Witter, M. P. (2009). The anatomy of memory: an interactive overview of the parahippocampal–hippocampal network. *Nature reviews neuroscience*, *10*(4), 272-282.

Vann, S. D., & Albasser, M. M. (2011). Hippocampus and neocortex: recognition and spatial memory. *Current opinion in neurobiology*, *21*(3), 440-445.

Varga, C., Golshani, P., & Soltesz, I. (2012). Frequency-invariant temporal ordering of interneuronal discharges during hippocampal oscillations in awake mice. Proceedings of the National Academy of Sciences, 109(40), E2726-E2734.

Vaz, A. P., Inati, S. K., Brunel, N., & Zaghloul, K. A. (2019). Coupled ripple

oscillations between the medial temporal lobe and neocortex retrieve human memory. Science, 363(6430), 975-978.

Villette V, Levesque M, Miled A, Gosselin B, Topolnik L (2017). Simple platform for chronic imaging of hippocampal activity during spontaneous behaviour in an awake mouse. Scientific Reports, 7, 43388.

Vorster, A. P., & Born, J. (2015). Sleep and memory in mammals, birds and invertebrates. *Neuroscience & Biobehavioral Reviews*, *50*, 103-119.

Wang, S. H., & Morris, R. G. (2010). Hippocampal-neocortical interactions in memory formation, consolidation, and reconsolidation. *Annual review of psychology*, *61*(1), 49-79.

Wang, T., & Xu, C. (2020). Three-photon neuronal imaging in deep mouse brain. *Optica*, *7*(8), 947-960.

Wei Z, Lin B-J, Chen T-W, Daie K, Svoboda K, Druckmann S. (2020). A comparison of neuronal population dynamics measured with calcium imaging and electrophysiology. PLoS Comput Biol 16(9): e1008198.

Wiener, S. I., Paul, C. A., & Eichenbaum, H. (1989). Spatial and behavioral correlates of hippocampal neuronal activity. *Journal of Neuroscience*, *9*(8), 2737-2763.

Wilson, M. A., & McNaughton, B. L. (1994). Reactivation of hippocampal ensemble memories during sleep. *Science*, *265*(5172), 676-679.

Wyss, J. M., Swanson, L. W., & Cowan, W. M. (1980). The organization of the fimbria, dorsal fornix and ventral hippocampal commissure in the rat. *Anatomy and embryology*, *158*(3), 303-316.

Xia, F., Richards, B. A., Tran, M. M., Josselyn, S. A., Takehara-Nishiuchi, K.,

& Frankland, P. W. (2017). Parvalbumin-positive interneurons mediate neocortical-hippocampal interactions that are necessary for memory consolidation. *Elife*, *6*, e27868.

Yang, Y., & Wang, J. Z. (2017). From structure to behavior in basolateral amygdala-hippocampus circuits. *Frontiers in neural circuits*, *11*, 86.

Zhou H, Neville K, Goldstein N, Kabu S, Kausar N, Ye R, Nguyen T, Gelwan N, Hyman B, Gomperts S (2019). Cholinergic modulation of hippocampal calcium activity across the sleep-wake cycle. Elife, 8, e39777.

국문요약

우리의 일상 생활에서는 다양한 경험이 다양한 환경에서 일어난다. 그 중 일부는 평생 지속되는 강렬한 경험이 되기도 하고, 다른 경험들은 기억도 되지 못하고 쉽게 잊혀진다. 이러한 기억의 선택적 저장에는, 경험의 입력 과정(encoding) 뿐 만 아니라 경험의 강화 (consolidation) 과정도 큰 영향을 끼친다. 해마의 sharp wave-ripples (SWRs) 와 그 구성 뉴런들은 장기 기억의 형성 과정을 연구하는 데에 큰 비중을 차지해왔다. 특히 이 뉴런의 신호들은 전기생리학적 방식으로 기록되고 연구되었다. 그러나, 이러한 신호들은 뉴런의 위치에 대한 정보가 부족하고 장기간에 걸쳐 같은 뉴런을 인식할 수 없기 때문에, 특정 환경에서 일어나는 SWRs이 어떠한 뉴런으로 구성되어있는지 연구하는 데에는 어려움이 있었다.

이 논문에서는, 해마의 SWRs을 구성하는 뉴런들을 시간적 측면 뿐 만 아니라 공간적 측면에서도 관찰하여, SWRs로 인해 강화되는 기억을 구성하는 뉴런들을 식별하고자 하였다. SWRs의 구성과 환경에 따른 구성의 변화를 알아보기 위해, 본 연구는 아래의 두 부분으로 나누어 진행되었다.

첫번째 부분에서는 전기생리학적 방법과 칼슘 이미징 방법을 통해, 자유롭게 움직이는 생쥐의 해마에서 발생하는 SWRs을 두 가지 방법으로 기록하고, 그 신호에 따라 변화하는 뇌세포의 활동을 알아보고자 한다. 이를 위하여 살아있는 동물에서 실시간으로 전기신호를 측정할 수 있는 초소형 기구를 만들고, 이를 단광자 칼슘 이미징 장치와 결합시켰다. 이러한 방식을 통해 해마의 SWRs을 전기생리학적 방식과 칼슘 신호의 두 가지 방식으로 기록하였다. 기록 결과, 해마의 뇌세포들의 활동성이 SWRs이 시작됨에 따라 증가하는 것이 확인되었다. 반면, SWRs이 방해된 경우에는 해마 뇌세포의 활동성 증가가 관찰되지 않았다. 이러한 결과는, SWRs을 구성하는 세포들이 기억 강화 과정에 영향을 미칠 수 있음을 암시한다.

두 번째 부분에서는, 해마 뉴런에서 얻어진 칼슘 신호들을 동물들의 실험 환경에

따라 비교하여 보았다. 동물들이 두 개의 다른 환경을 경험하고 있는 동안, 해마에서 발생하는 SWRs 신호가 실시간으로 기록되었다. 그 결과, 동물들이 처한 환경에 따라서, 서로 다른 해마 뉴런으로 구성된 그룹들이 SWRs을 구성하고 있다는 것을 발견하였다. 즉, 해마의 SWRs들은 여러 뉴런의 신호들로 이루어져 있으나 그 각각을 구성하는 뉴런은 경험의 환경에 따라 달라질 수 있음을 보여준다. 또한 이러한 결과는, 기억의 재생 (replay)과 그 구성 뉴런을 식별하기 위한 신호의 해독 (decoding) 과정에서의 정확성을 높이는 데에 기여할 수 있음을 보여준다.

정리하면, 이 논문을 통하여, 해마에 저장되어 있는 기억을 구성하는 뉴런들을 식별하기 위한 실험 도구의 개발부터 그 결과 발견한 과학적인 내용의 분석에 이르기까지의 단계들을 포괄적으로 기술하고 소개하고자 한다.

주요어: 학습과 기억, 해마, 지역장전위, SWRs, 전기생리신호 기록, 칼슘 신호 기록

학번: 2014-25058